

See discussions, stats, and author profiles for this publication at: <https://www.researchgate.net/publication/280918806>

# Crystal Structure of Isotactic Poly((R,S)-3-methyl-1-pentene)

ARTICLE *in* MACROMOLECULES · JULY 2015

Impact Factor: 5.8

---

READS

48

7 AUTHORS, INCLUDING:



Claudio De Rosa

University of Naples Federico II

207 PUBLICATIONS 5,617 CITATIONS

[SEE PROFILE](#)



Giuseppe Leone

Italian National Research Council

38 PUBLICATIONS 225 CITATIONS

[SEE PROFILE](#)



Antonella Caterina Boccia

Italian National Research Council

35 PUBLICATIONS 249 CITATIONS

[SEE PROFILE](#)

## Crystal Structure of Isotactic Poly((R,S)-3-methyl-1-pentene)

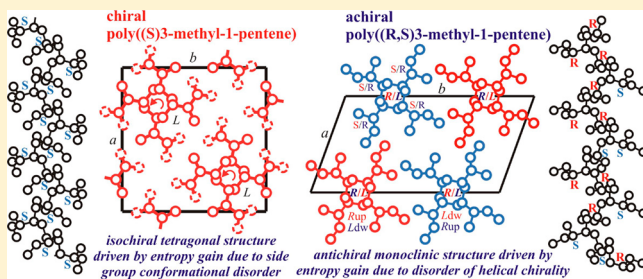
Claudio De Rosa,\*<sup>†</sup> Finizia Auriemma,<sup>†</sup> Chiara Santillo,<sup>†</sup> Rocco Di Girolamo,<sup>†</sup> Giuseppe Leone,<sup>‡</sup> Antonella Caterina Boccia,<sup>‡</sup> and Giovanni Ricci<sup>‡</sup>

<sup>†</sup>Dipartimento di Scienze Chimiche, Università di Napoli Federico II, Complesso Monte S. Angelo, Via Cintia, I-80126 Napoli, Italy

<sup>‡</sup>CNR-Istituto per lo Studio delle Macromolecole (ISMAC), Via Bassini 15, I-20133 Milano, Italy

### S Supporting Information

**ABSTRACT:** The synthesis and the crystal structure of isotactic poly((R,S)-3-methyl-1-pentene) (iP(R,S)3MP) are presented. The synthetic strategy based on hydrogenation of isotactic 1,2-poly(*E*-3-methyl-1,3-pentadiene) has allowed for the preparation of a purely random copolymer of the two enantiomeric (*R*)- and (*S*)-3-methyl-1-pentene monomers. X-ray diffraction analysis and conformational and packing energy calculations have shown that chains of iP(R,S)3MP are in 4/1 helical conformation and are packed in a monoclinic unit cell with parameters  $a = 10.02 \text{ \AA}$ ,  $b = 18.48 \text{ \AA}$ ,  $c = 6.87 \text{ \AA}$ , and  $\gamma = 109.9^\circ$  according to the space group  $P2_1/b$  or  $P2_1$ . A high degree of disorder is present in the crystals due to the random enchainment of the enantiomeric *R* and *S* monomeric units, whose chirality influences the handedness of the helical chains and the conformation assumed by the lateral groups. Disorder in the conformation of the lateral groups is also present. The crystal structure of the random copolymer iP(R,S)3MP is different from the tetragonal structure of the pure enantiomer homopolymer iP(S)3MP. This is due to different entropic effects, related to the presence of different types of disorder included in the crystals that drive crystallization in different packing modes. The crystal structure of iP(R,S)3MP provides an example of the effect of the chirality of side groups on the crystal packing and is an example of symmetry breaking in the structures of polymers.



## INTRODUCTION

The crystal structure, the polymorphism, and the crystallization behavior of chiral polyolefins, bearing chiral side groups, have been extensively investigated to study the effect of the presence of chiral atoms on the conformation of macromolecules and crystal packing<sup>1–3</sup> and, more recently, in connection with a phenomenon described as a macromolecular amplification of chirality.<sup>4</sup>

Isotactic poly(3-methyl-1-pentene) (iP3MP) is a chiral branched poly( $\alpha$ -olefin) with a “true” asymmetric atom on the side chain of the monomeric unit. The polymerization of the chiral monomer (*S*)-3-methyl-1-pentene ((*S*)3MP) with stereoselective Ziegler–Natta or metallocene catalysts produces a chiral isotactic polymer, poly((*S*)-3-methyl-1-pentene) (iP-*(S)*3MP),<sup>5–7</sup> whereas the polymerization of the racemic mixture (*R,S*)-3MP gives an isotactic copolymer poly((*R,S*)-3-methyl-1-pentene) (iP(*R,S*)-3MP), where the two enantiomeric monomers (*S*)-3MP and (*R*)-3MP should be randomly enchainable.<sup>6</sup> Both chiral iP(*S*)-3MP and achiral iP(*R,S*)-3MP are crystalline<sup>3,7</sup> thanks to the isotactic configuration of the chains and, in the case of iP(*R,S*)-3MP, in spite of the configurational disorder due to the statistical enchainment of monomeric units of opposite *R* and *S* chirality.<sup>7</sup>

The crystal structure of iP(*S*)-3MP is characterized by chains in 4/1 helical conformation, and only left-handed helices are included in the tetragonal unit cell according to the space group  $I4_1$ .<sup>3</sup> The left-handed helix of iP(*S*)-3MP is favored over the

right-handed helix because the lateral groups of left-handed helices assume statistically two conformations of minimum energy, providing a gain in entropy.<sup>3,8–10</sup> In the case of the achiral iP(*R,S*)-3MP the random succession of enantiomeric monomeric units induces different crystallization behavior, but the crystal structure is still unknown.

In this paper we report the crystal structure of iP(*R,S*)-3MP prepared by hydrogenation of isotactic 1,2-poly(*E*-3-methyl-1,3-pentadiene) (iP3MPD12). The synthetic strategy guarantees that a purely statistical copolymer of the two enantiomeric monomeric units with compensation of chirality is obtained. In fact, the polymerization of the racemic mixture of the 3-methyl-1-pentene monomer (*R,S*)-3MP with stereospecific Ziegler–Natta catalyst produces a mixture of copolymers that was separated into fractions having optical activity of opposite sign,<sup>6</sup> indicating that copolymers of the two enantiomeric monomeric units, with prevalence of *S* or *R* monomeric units in the optically active polymers were obtained.<sup>6</sup> We show that the crystal structure of the purely random iP(*R,S*)-3MP is different from that of the chiral iP(*S*)-3MP, and this is a result of entropic effects related to the presence of different types of disorder included in the crystals.

Received: May 1, 2015

Revised: July 8, 2015

Published: July 27, 2015



## ■ EXPERIMENTAL SECTION

Samples of the precursor isotactic 1,2-poly(*E*-3-methyl-1,3-pentadiene) (iP3MPD12) were prepared with a new class of catalysts based on cobalt phosphine complexes of the type  $\text{CoCl}_2(\text{PRPh}_2)_2$  (with R = methyl, ethyl, *n*-propyl, isopropyl, cyclohexyl),<sup>11</sup> as described in ref 12 (see [Supporting Information](#)). Samples of the random achiral copolymer iP(*R,S*)3MP were prepared by hydrogenation of iP3MPD12 with *p*-toluenesulfonyl hydrazide<sup>13</sup> (see [Supporting Information](#)). The molecular structures of the samples of iP3MPD12 and iP(*R,S*)3MP were characterized by FT-IR, <sup>1</sup>H and <sup>13</sup>C NMR, DSC, and GPC analyses. Both samples iP3MPD12 and iP(*R,S*)3MP present high molecular mass (around 90 000 g/mol) and are highly isotactic, with concentration of isotactic triad mm higher than 90%. Therefore, according to the synthetic strategy, the high isotacticity of iP3MPD12 ([mm] ≥ 90%) is preserved after hydrogenation. The isotacticity of iP(*R,S*)3MP has been also directly probed by performing some mono- and two-dimensional solution NMR experiments as reported in the [Supporting Information](#).

Unoriented films used for structural analysis were obtained by compression molding of as-polymerized samples. The powders samples were heated at  $\approx 240$  °C between perfectly flat brass plates under a press at very low pressure, kept at  $\approx 240$  °C for 5 min, and cooled to room temperature. Crystalline oriented fibers were obtained by extrusion of melt in a syringe and stretching. Details of X-ray diffraction analysis, calculations of structure factors, and conformational and packing energies are reported in the [Supporting Information](#).

## ■ RESULTS AND DISCUSSION

The X-ray powder diffraction profiles of the as-polymerized sample and of the melt-crystallized compression-molded sample of iP( $R,S$ )3MP are shown in Figure 1. Both diffraction

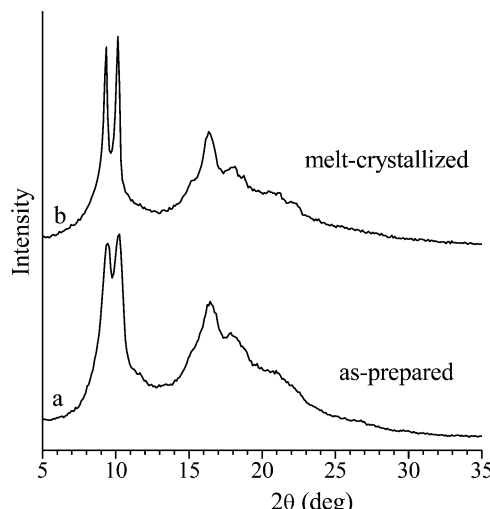


**Figure 1.** X-ray powder diffraction profiles of as-prepared (a) and melt-crystallized compression-molded sample (b) of iP(*R,S*)3MP.

profiles are characterized by two strong, sharp, and very close reflections at  $2\theta = 9.5^\circ$  and  $10.4^\circ$  and a strong reflection at  $2\theta = 16.6^\circ$ . The diffraction profile of the melt-crystallized sample presents sharper reflections and, in particular, the two close reflections at  $2\theta = 9.5^\circ$  and  $10.4^\circ$  are more separated and clearly resolved. The DSC heating curve of the as-polymerized sample of iP(*R,S*)3MP, the successive cooling curve from the melt to low temperature, and the successive heating curve of the melt-crystallized sample are reported in Figure 2. The as-polymerized sample is crystalline with melting temperature of  $198^\circ\text{C}$  and crystallizes from the melt by cooling at  $10^\circ\text{C}/\text{min}$ .

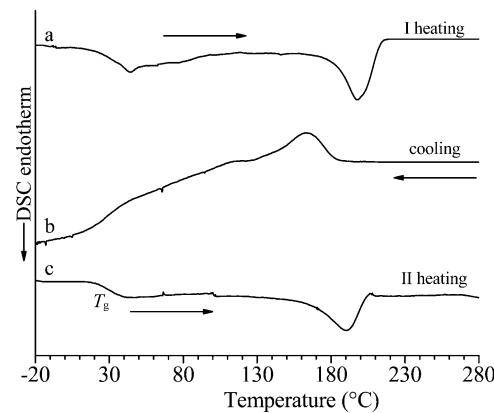


**Figure 2.** DSC curves of as-polymerized sample of iP(*R,S*)3MP recorded during heating (a), successive cooling from the melt down to low temperature (b), and successive heating of the melt-crystallized sample (c). All DSC curves have been recorded at scanning rate of 10 °C/min.

at nearly 160 °C. A glass transition temperature of about 43 °C has been evaluated in both heating and cooling DSC scans (Figure 2).

It is worth noting that the X-ray diffraction profile of Figure 1 of the achiral iP(R,S)3MP is different from that of the chiral iP(S)3MP (see Figure 3 of ref 7), which is characterized at low values of  $2\theta$  by a single strong reflection at  $2\theta = 9.3^\circ$  (see Figures 3b and 4 of ref 7). This indicates that the crystal structure of the copolymer of the two enantiomeric monomeric units iP(R,S)3MP is different from that of the enantiopure iP(S)3MP,<sup>3</sup> which is characterized by chains in 4/1 helical conformation packed in a tetragonal unit cell with axis  $a = b = 13.35 \text{ \AA}$  and  $c = 6.80 \text{ \AA}$ , according to the space group  $I4_1$ .<sup>3</sup> Only left-handed 4/1 helices are included in the tetragonal unit cell since the left-handed helix of iP(S)3MP is favored over the right-handed one because of the chirality of the lateral group. The crystal structure of iP(S)3MP has been described in terms of statistical disorder of the optically active chiral side groups, which assume, in the left-handed chains, randomly two different almost isoenergetic conformations, providing a gain in entropy.<sup>3,10</sup>

Oriented fibers of  $iP(R,S)3MP$  have been obtained by extrusion of the melt and contemporarily stretching. The X-ray fiber diffraction pattern of  $iP(R,S)3MP$  is reported in Figure 3. All the reflections observed in the fiber pattern of Figure 3 and in the powder diffraction profiles of Figure 1b are listed in

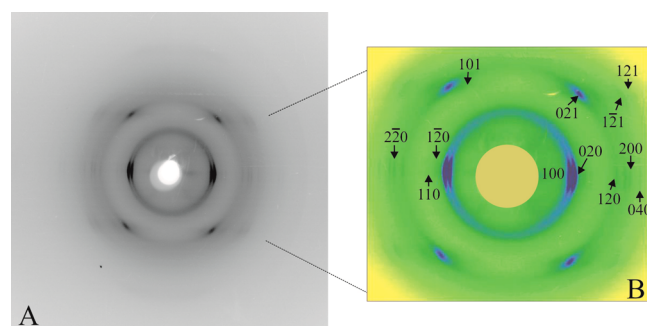


**Figure 3.** X-ray fiber diffraction pattern of oriented fiber of iP(*R,S*)3MP (A). The Miller indices of the most intense reflections in (A) are indicated in (B) in a false color scale.

**Table 1.** Diffraction Angles ( $2\theta$ ), Bragg Distances ( $d$ ), Cylindrical Reciprocal Coordinates ( $\xi$  and  $\zeta$ ), and Intensities ( $I_0$ ) of the Reflections Observed on the Layer Lines  $l$  of the X-ray Fiber Diffraction Pattern of iP(R,S)3MP of Figure 3, Compared with the Diffraction Angles, Bragg Distances, and Intensities Observed in the X-ray Power Diffraction Profile of Figure 1b<sup>a</sup>

fiber diffraction pattern (Figure 3)							powder diffraction profile (Figure 1b)			
$2\theta$ (deg)	$d$ (Å)	$\xi$ (Å $^{-1}$ )	$\zeta$ (Å $^{-1}$ )	$l$	$I_0$ <sup>b</sup>	$hkl$	$2\theta$ (deg)	$d_0$ (Å)	$I_0$	$hkl$
9.4	9.43	0.106	0	0	vs	100	9.3	9.51	41	100
10.2	8.69	0.115	0	0	vs	020	10.2	8.67	37	020
11.7	7.53	0.133	0	0	vw	1̄20	15.1	5.87	16	101
12.8	6.91	0.145	0	0	vw	110	16.4	5.40	35	021
16.8	5.28	0.189	0	0	vw	120	18.2	4.87	19	1̄21, 2̄20
18.1	4.89	0.204	0	0	vvw	2̄20	18.8	4.72	15	200
18.9	4.70	0.213	0	0	w	200	21.2	4.19	21	121
20.5	4.34	0.230	0	0	vw	040	22.1	4.02	12	201
25.3	3.52	0.284	0	0	vvw	140				
26.3	3.39	0.295	0	0	vvw	3̄20				
15.6	5.70	0.098	0.1456	1	w	101				
16.6	5.34	0.117	0.1456	1	s	021				
18.3	4.85	0.146	0.1456	1	w	1̄21				
21.2	4.20	0.188	0.1456	1	vw	121				
22.0	4.03	0.201	0.1456	1	w	201				

<sup>a</sup>The Miller indices  $hkl$  of reflections for a monoclinic unit cell with parameters  $a = 10.02$  Å,  $b = 18.48$  Å,  $c = 6.87$  Å, and  $\gamma = 109.9^\circ$  are also indicated. <sup>b</sup>vs = very strong; s = strong; w = weak; vw = very weak; vvw = very very weak.

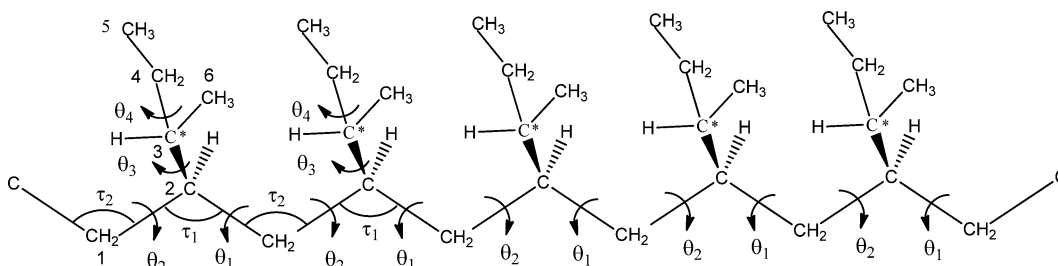


**Figure 4.** Portion of the chain of iP(S)3MP or iP(R)3MP used in the conformational energy calculations with definition of the torsion angles  $\theta_1$ ,  $\theta_2$ ,  $\theta_3$ , and  $\theta_4$  and the bond angles  $\tau_1$  and  $\tau_2$ . The torsion angle  $\theta_3$  is defined with respect to the carbon of the  $\text{CH}_2$  group of the ethyl group:  $\theta_3 = \text{C}4-\text{C}3^*-\text{C}2-\text{C}1$ . The torsion angle  $\theta_4$  is defined with respect to the methyl group of the ethyl group:  $\theta_4 = \text{C}5-\text{C}4-\text{C}3^*-\text{C}2$ .

**Table 1.** It is apparent that the two strong reflections at  $2\theta = 9.5^\circ$  and  $10.4^\circ$  observed in the powder profile (Figure 1b) are equatorial reflections (Figure 3), whereas the strong reflection at  $2\theta = 16.6^\circ$  is a first layer line reflection (Figure 3 and Table 1). From the fiber pattern the value of the chain axis  $c = 6.87$  Å has been evaluated for the chains of iP(R,S)3MP.

The value of the chain axis of  $6.87$  Å of iP(R,S)3MP is almost identical to the value of the chain axis of  $6.80$  Å found for the chiral iP(S)3MP.<sup>3</sup> This indicates that chains of the achiral iP(R,S)3MP assume the same 4/1 helical conformation of the chains of the chiral iP(S)3MP.<sup>3</sup> The reflections observed in the fiber pattern of Figure 3 and the powder diffraction profile of Figure 1b of iP(R,S)3MP are all accounted for by a monoclinic unit cell with parameters  $a = 10.02$  Å,  $b = 18.48$  Å,  $c = 6.87$  Å, and  $\gamma = 109.9^\circ$ . The calculated density with two chains in the cell is  $0.932$  g/cm $^3$ , in agreement with the experimental density of  $0.878$  g/cm $^3$  measured at  $25^\circ\text{C}$  by flotation on a sample with X-ray crystallinity of  $\approx 47\%$  (the crystalline density is  $0.885$  g/cm $^3$  evaluated from the experimental density of  $0.878$  g/cm $^3$  and the experimental density of the amorphous sample of  $0.868$  g/cm $^3$ ). The indices  $hkl$  of the reflections according to this monoclinic unit cell are reported in Table 1.

The indexing of the observed reflections indicates, disregarding in a first approximation the very weak 110 reflection observed in the fiber pattern, the systematic absence

of  $hk0$  reflections with  $k$  odd. This suggests that a possible space group, compatible with the presence of two chains in the unit cell, could be  $P2_1/b$ . As a consequence of the choice of this monoclinic space group, the 4/1 helical symmetry of the chains is not maintained in the lattice as crystallographic symmetry, as instead occurs for the chiral iP(S)3MP.<sup>3,10</sup> The chains can be positioned in the unit cell with their chain axes coincident with the crystallographic  $2_1$  axes of the space group  $P2_1/b$ .

Possible models of packing of 4/1 helical chains in the monoclinic unit cell have been found performing calculations of the conformational energy and packing energy for the space group  $P2_1/b$ . The calculations of the conformational energy have been performed on a portion of isolated chains of iP(R)3MP, iP(S)3MP, and iP(R,S)3MP shown in Figure 4, by application of the equivalence principle<sup>10</sup> to successive constitutional units by assuming a line repetition group  $s(M/N)$  for the polymer chain. As a consequence, the sequence of the torsion angles in the main chain is of the kind ... $\theta_1\theta_2\theta_1\theta_2$ ... (Figure 4) (see Supporting Information). The conformational energy maps for chains of iP(R)3MP and iP(S)3MP as a function of  $\theta_1$  and  $\theta_2$  are shown in Figure 5. In these maps for each pair of  $\theta_1$  and  $\theta_2$ , the positions of the side groups, defined by the torsion angles  $\theta_3$  and  $\theta_4$ , were varied in step of  $10^\circ$  of  $\theta_3$  and  $\theta_4$ , to place them in the minimum-energy position corresponding to that pair of  $\theta_1$  and  $\theta_2$ . Two energy minima

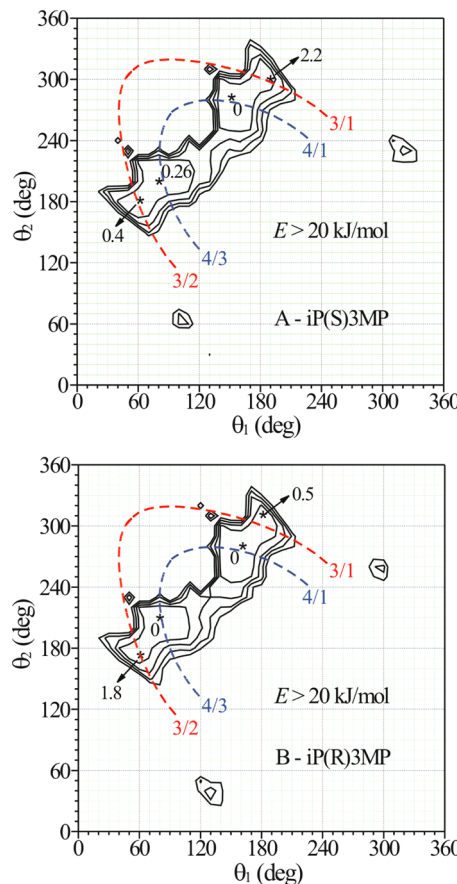


**Figure 5.** Maps of the conformation energy of iP(S)3MP (A) and iP(R)3MP (B) as a function of  $\theta_1$  and  $\theta_2$  with  $\theta_3$  and  $\theta_4$  scanned every  $10^\circ$  in the  $s(M/N)$  line repetition group for  $\tau_1 = 111^\circ$  and  $\tau_2 = 113^\circ$ . The curves are reported at intervals of 5 kJ/mol of monomeric units with respect to the absolute minimum of the maps assumed as zero. The values of the energy corresponding to the minima (\*) are also reported. The dashed curves represent the loci of points of couples of torsion angles  $\theta_1$  and  $\theta_2$  corresponding to the  $s(4/1)$  and  $s(3/1)$  helical conformations.

are present in both maps of Figure 5 in the region  $\theta_1 \approx G^+$ ,  $\theta_2 \approx T$ , or  $\theta_1 \approx T$ ,  $\theta_2 \approx G^-$ . The values of torsion angles and of the relative energies are reported in Table 2.

The loci of points corresponding to the  $s(4/1)$  and  $s(3/1)$  helical symmetries, with values of the unit twist  $t = 2\pi N/M$  of  $90^\circ$  and  $120^\circ$ , respectively, are also reported in the maps of Figure 5.<sup>10</sup> The absolute energy minimum is close to conformations with  $4/1$  helical symmetry, while the relative minimum is close to the dashed line corresponding to conformations with  $3/1$  symmetry. However, no polymorphic form with  $s(3/1)$  helical chains has been observed until now for iP(S)3MP or iP(R,S)3MP. The conformations with  $4/1$  helical symmetry correspond to isodistortions for  $\theta_1$  and  $\theta_2$  from the precise *gauche* and *trans* values due to the bulkiness of the lateral groups.<sup>10</sup>

According to this geometrical and energy analysis, models of the chains of iP(S)3MP, iP(R)3MP, and of the random copolymer iP(R,S)3MP are built with the values of the dihedral angles along the main chain of  $\theta_1 = 150^\circ$ ,  $\theta_2 = -80^\circ$  (or  $\theta_1 = 80^\circ$ ,  $\theta_2 = -160^\circ$ ) (Table 2). The possible conformations of the side groups have been evaluated by calculating the conformational energy of the  $4/1$  right-handed helix for  $\theta_1 = 150^\circ$ ,  $\theta_2 = -80^\circ$  (or the left-handed helix for  $\theta_1 = 80^\circ$ ,  $\theta_2 = -160^\circ$ ),

**Table 2.** Values of Torsion Angles of the Backbone  $\theta_1$  and  $\theta_2$ , and of the Lateral Groups  $\theta_3$  and  $\theta_4$  (Figure 4) Corresponding to the Minima of the Conformational Energy Found in Maps of Figure 5 of iP(S)3MP and iP(R)3MP, and Values of the Corresponding Energy  $E$  Scaled with Respect to the Absolute Minimum of the Maps Assumed as Zero<sup>a</sup>

$\theta_1$ (deg)	$\theta_2$ (deg)	$\theta_3$ (deg)	$\theta_4$ (deg)	$E$ (kJ/ mol mu)	helix symmetry
iP(S)3MP					
150	-80	50	170	0	4/1 right-handed (up)
80	-160	-160	170	0.26	4/1 left-handed (down)
-170	-60	60	170	2.25	3/1 right-handed (up)
60	180	180	160	0.36	3/1 left-handed (down)
iP(R)3MP					
160	-80	-70	-160	0.04	4/1 right-handed (up)
80	-150	80	-160	0	4/1 left-handed (down)
180	-50	-60	-160	0.55	3/1 right-handed (up)
60	170	60	-170	1.83	3/1 left-handed (down)

<sup>a</sup>The “up” or “down” orientations of the chain models are also indicated. In our modeling right-handed chains are built “up” and left-handed chains are built “down”.

varying the torsion angles  $\theta_3$  and  $\theta_4$ . The conformational energy maps of iP(S)3MP and iP(R)3MP as a function of  $\theta_3$  and  $\theta_4$  for these fixed values of  $\theta_1$  and  $\theta_2$  are reported in Figure 6. The values of torsion angles and of the relative energies of minima are reported in Table 3. It is apparent that for iP(S)3MP low-energy minima are obtained for only one possible value of  $\theta_3$ , that is,  $\theta_3 \approx T$  for the left-handed  $4/1$  helix and  $\theta_3 \approx G^+$  for the right-handed  $4/1$  helix, while  $\theta_4$  may assume different values around  $T$  and  $G^+$  (Table 3). For the left-handed helix the two minima corresponding to  $\theta_3 \approx T$  and  $\theta_4 \approx G^+$  are isoenergetic, whereas for the right-handed  $4/1$  helix a deep energy minimum is obtained only for one value of  $\theta_4$ , that is, for  $\theta_3 \approx G^+$  and  $\theta_4 \approx T$ . Analogously, for iP(R)3MP low-energy minima are obtained for  $\theta_3 \approx G^+$  for the left-handed  $4/1$  helix and  $\theta_3 \approx G^-$  for the right-handed  $4/1$  helix, while  $\theta_4$  may assume different values around  $T$  and  $G^-$  (Table 3). Moreover, for the right-handed helix the two minima corresponding to  $\theta_3 \approx G^-$  and two different values of  $\theta_4$  at  $\theta_4 \approx T$  and  $\theta_4 \approx G^-$  are isoenergetic, whereas for the left-handed  $4/1$  helix a deep energy minimum is obtained only for one value of  $\theta_4$ , that is, for  $\theta_3 \approx G^+$  and  $\theta_4 \approx T$ . The three possible conformations of left- and right-handed  $4/1$  helices of iP(S)3MP (two for the left-handed and one for the right-handed chain) and the three possible conformations of left- and right-handed  $4/1$  helices of iP(R)3MP (two for the right-handed and one for the left-handed chain) are shown in Figure 7. The six models of possible conformations are defined iP(S)3MP-L-TG<sup>+</sup> (left-handed  $4/1$  chain of iP(S)3MP with  $\theta_3 = T$  and  $\theta_4 = G^+$ , Figure 7A), iP(S)3MP-L-TT (left-handed  $4/1$  chain of iP(S)3MP with  $\theta_3 = T$  and  $\theta_4 = T$ , Figure 7B), iP(S)3MP-R-G<sup>+</sup>T (right-handed  $4/1$  chain of iP(S)3MP with  $\theta_3 = G^+$  and  $\theta_4 = T$ , Figure 7C), iP(R)3MP-R-G<sup>-</sup>G<sup>-</sup> (right-handed  $4/1$  chain of iP(R)3MP with  $\theta_3 = G^-$  and  $\theta_4 = G^-$ , Figure 7D), iP(R)3MP-R-G<sup>-</sup>T (right-handed  $4/1$  chain of iP(R)3MP with  $\theta_3 = G^-$  and  $\theta_4 = T$ , Figure 7E), and iP(R)3MP-L-G<sup>+</sup>T (left-handed  $4/1$  chain of iP(R)3MP with  $\theta_3 = G^+$  and  $\theta_4 = T$ , Figure 7F) (Table 3).

Besides these six low-energy models, other two models of conformation of slight higher energy are included in Table 3 and Figure 7. These models correspond to the isolated minima

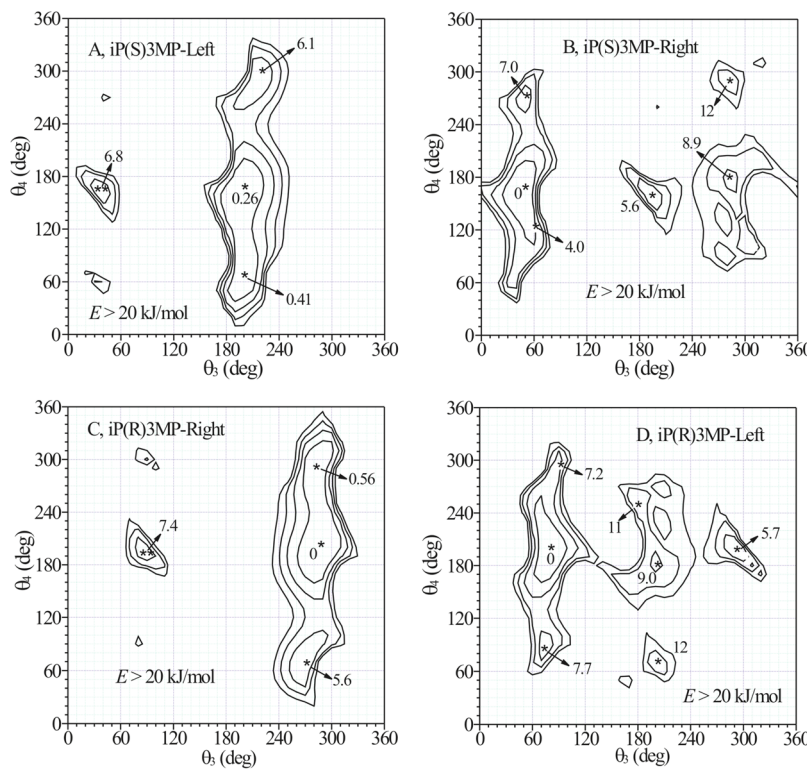


**Figure 6.** Maps of the conformational energy of iP(S)3MP (A, B) and iP(R)3MP (C, D) for backbone torsion angles  $\theta_1 = 150^\circ$ ,  $\theta_2 = -80^\circ$  (right-handed helix) (B, C), or  $\theta_1 = 80^\circ$ ,  $\theta_2 = -160^\circ$  (left-handed helix) (A, D), corresponding to the 4/1 left-handed or right-handed helix, as a function of the torsion angles  $\theta_3$  and  $\theta_4$  that define the conformation of the lateral groups. The curves are reported at intervals of 5 kJ/mol of monomeric units with respect to the absolute minimum of the maps assumed as zero. The values of energy of the minima (\*) are also reported.

of the energy maps of Figure 6A,C (indicated with a double star) of energy  $\approx 7$  kJ/mol mu higher than the absolute minima. These local minima correspond for iP(S)3MP to the model iP(S)3MP-L-G<sup>+</sup>T (Figure 7C') of a left-handed 4/1 helix with  $\theta_3 \approx G^+$  and  $\theta_4 \approx T$  (Figure 6A) and for iP(R)3MP to the model iP(R)3MP-R-G<sup>+</sup>T (Figure 7F') of a right-handed 4/1 helix with  $\theta_3 \approx G^+$  and  $\theta_4 \approx T$  (Figure 6C). It is worth noting that the model iP(S)3MP-L-G<sup>+</sup>T (Figure 7C') has the same conformation as the model of absolute energy minimum for the iP(R)3MP chain (iP(R)3MP-L-G<sup>+</sup>T, Figure 7F) but opposite chirality of the lateral groups, and the model iP(R)3MP-R-G<sup>+</sup>T (Figure 7F') has the same conformation as the model of absolute energy minimum for the iP(S)3MP chain (iP(S)3MP-R-G<sup>+</sup>T, Figure 7C), but opposite chirality of the lateral groups. The high energy of the conformational models of Figure 7C', F' evidences the tendency of the chiral side groups to influence the chirality and the conformation of the helical chains, by destabilizing the internal energy of a helix of a given chirality by about 7 kJ/mol mu.

It is also worth mentioning that the isotactic chains of iP(R)3MP and iP(S)3MP may assume two different “up” and “down” orientations, characterized by the C–C bonds connecting the side chains to the tertiary carbon atoms of the backbone pointing in the positive direction of the z-axis (coincident with the chain axis) defining an “up” chain, or the negative direction, defining a “down” chain. In the models of Figure 7, regardless of chirality of side groups, the left-handed chains are drawn down, whereas the right-handed chains are drawn up.

Similar calculations have been performed for model chains of copolymer iP(R,S)3MP, and similar results as in Table 3 have

been obtained for the lowest energy conformations. For left-handed 4/1 helix of iP(R,S)3MP the side groups of the R monomeric units assume conformation with  $\theta_3 \approx G^+$  and  $\theta_4 \approx T$  (as in the model F of Table 3), and the side groups of the S monomeric units assume conformation with  $\theta_3 \approx T$  and  $\theta_4 \approx T$  (as in the model B of Table 3), whereas for right-handed 4/1 helix of iP(R,S)3MP the side groups of the S monomeric units assume conformation with  $\theta_3 \approx G^+$  and  $\theta_4 \approx T$  (as in the model C of Table 3), and the side groups of the R monomeric units assume conformation with  $\theta_3 \approx G^-$  and  $\theta_4 \approx T$  (as in the model E of Table 3). Models of left-handed and right-handed 4/1 helical conformation of the copolymer iP(R,S)3MP, where successive R and S monomeric units assume these conformations are shown in Figure 8. Although other conformations for the S and R side groups in consecutive monomeric units along the chain of iP(R,S)3MP would be also possible at low cost of conformational energy, those of Figure 8 correspond to the energy minima.

It is worth noting that for the low-energy conformers of R units in a left-handed 4/1 helix with  $\theta_3 \approx G^+$  and  $\theta_4 \approx T$  (model F of Table 3 and Figure 7F) and S units in a right-handed 4/1 helix with  $\theta_3 \approx G^+$  and  $\theta_4 \approx T$  (model C of Table 3 and Figure 7C), the ethyl groups are in a gauche arrangement to both the CH<sub>2</sub> groups of the backbone ( $\theta_3 \approx G^+$ ). For the low-energy conformers of S units in a left-handed 4/1 helix with  $\theta_3 \approx T$  and  $\theta_4 \approx T$  (model B of Table 3 and Figure 7B) and R units in a right-handed 4/1 helix with  $\theta_3 \approx G^-$  and  $\theta_4 \approx T$  (model E of Table 3 and Figure 7E), the methyl groups bonded to the chiral carbon are in a gauche arrangement to both the CH<sub>2</sub> groups of the backbone (the ethyl groups are in trans  $\theta_3 \approx T$  and gauche  $\theta_3 \approx G^-$ , respectively, to one of the

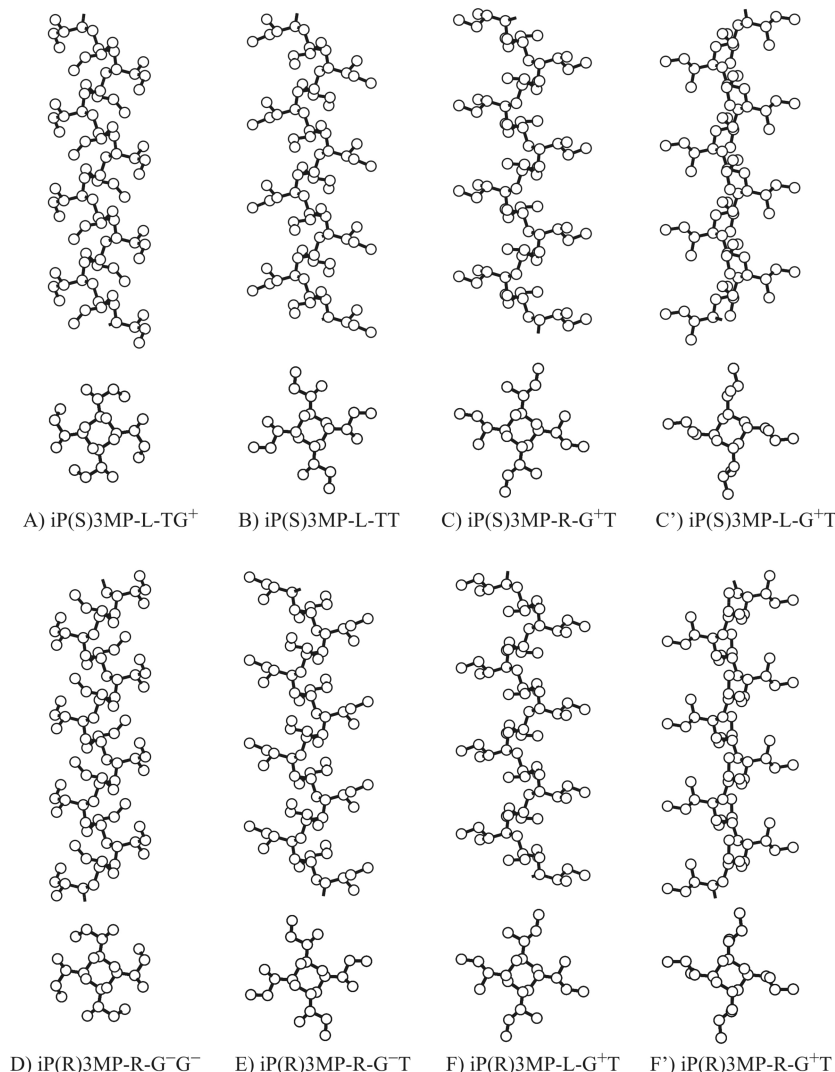


**Figure 7.** Height models of possible conformations of the chains of iP(S)3MP (A–C, C') and iP(R)3MP (D–F, F') found by calculations of conformational energy of Figures 5 and 6. The models correspond to the conformations defined in Table 3. Chains of models A, B, C', and F are “down”, and chains of models C, D, E, and F' are “up”.

**Table 3. Height Models of Conformations of the Chains of iP(S)3MP and iP(R)3MP Corresponding to the Minima of the Conformational Energy Found in the Maps of Figure 6<sup>a</sup>**

model of Figure 7	$\theta_1$ (deg)	$\theta_2$ (deg)	$\theta_3$ (deg)	$\theta_4$ (deg)	E (kJ/mol mu)	helix symmetry	model
iP(S)3MP							
A	80	-160	-160	70	0.41	4/1 left-handed	iP(S)3MP-L-TG <sup>+</sup> (down)
B	80	-160	-160	170	0.26	4/1 left-handed	iP(S)3MP-L-TT (down)
C	150	-80	50	170	0	4/1 right-handed	iP(S)3MP-R-G <sup>+</sup> T (up)
C'	80	-160	40	160	6.82	4/1 left-handed	iP(S)3MP-L-G <sup>+</sup> T (down)
iP(R)3MP							
D	160	-80	-80	-70	0.56	4/1 right-handed	iP(R)3MP-R-G <sup>-</sup> G <sup>-</sup> (up)
E	160	-80	-70	-160	0	4/1 right-handed	iP(R)3MP-R-G <sup>-</sup> T (up)
F	80	-150	80	-160	0	4/1 left-handed	iP(R)3MP-L-G <sup>+</sup> T (down)
F'	160	-80	90	-170	7.37	4/1 right-handed	iP(R)3MP-R-G <sup>+</sup> T (up)

<sup>a</sup>The values of torsion angles of the lateral groups  $\theta_3$  and  $\theta_4$  correspond to the minima of the maps of Figure 6 calculated with the constant values of the backbone torsion angles  $\theta_1$  and  $\theta_2$  found in the maps of Figure 5. The values of the conformational energy E are scaled with respect to the absolute minimum of the maps of Figures 5 and 6 assumed as zero. The labels A–F correspond to the model of Figure 7. In the symbols of models iP(R)3MP-X-YZ or iP(S)3MP-X-YZ, the label X (R or L) indicates right-handed (R) or left-handed (L) 4/1 helix, and the labels Y and Z (= T, G<sup>+</sup>, or G<sup>-</sup>) indicate the value of the torsion angle  $\theta_3$  and  $\theta_4$ , respectively.

two CH<sub>2</sub> groups of the backbone). The double gauche arrangement of ethyl and methyl groups is shown in the

Newman's projections in Figures 8A',B' and 8A'',B'', respectively.

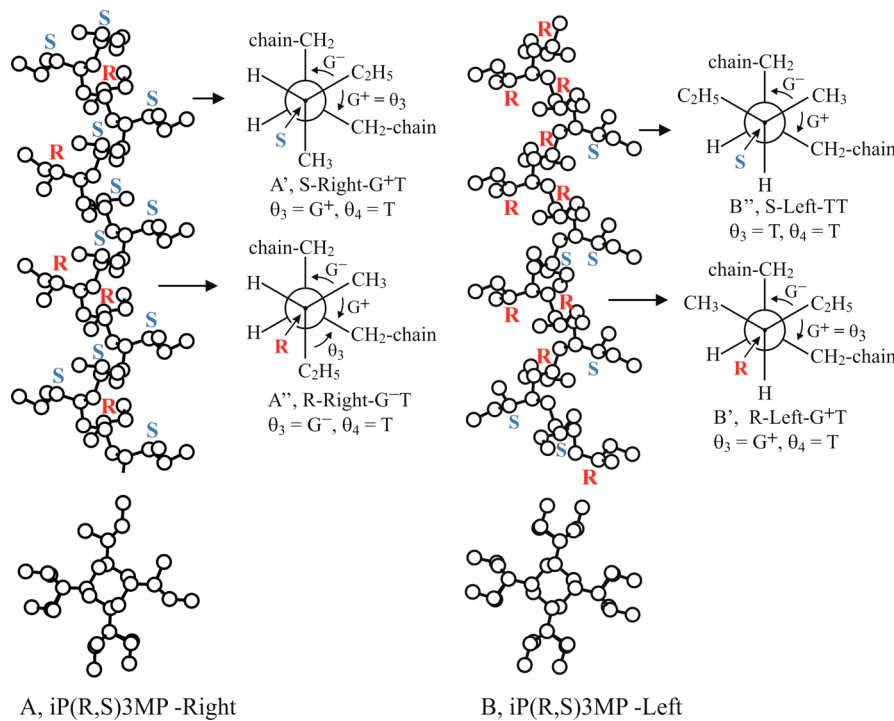


**Figure 8.** Models of right-handed and left-handed 4/1 helical conformation of the copolymer iP(R,S)3MP, where the side groups of successive R and S monomeric units assume statistically the lowest energy conformations of Figure 7. (A) iP(R,S)3MP chain in 4/1 right-handed helical conformation bearing S units with  $\theta_3 \approx G^+$ ,  $\theta_4 \approx T$  (A'), and R units with  $\theta_3 \approx G^-$ ,  $\theta_4 \approx T$  (A''). (B) iP(R,S)3MP chain in 4/1 left-handed helical conformation bearing R monomeric units with  $\theta_3 \approx G^+$ ,  $\theta_4 \approx T$  (B') and S units with  $\theta_3 \approx T$ ,  $\theta_4 \approx G^+$  (B''). The double gauche arrangements of ethyl and methyl groups are indicated in the Newman's projections of A', B' and A'', B'', respectively.

These results indicate that the random enchainment of S and R monomeric units in iP(R,S)3MP and the compensation of chirality make the left-handed and right-handed 4/1 helices equivalent because low-energy conformations of the chiral lateral groups are possible for both left-handed and right-handed helices (Table 3) and explain the experimental X-ray diffraction data that indicate a packing of enantiomorphous helices, according to the centrosymmetric space group  $P2_1/b$ , rather than an isomorphous packing, as in the case of iP(S)3MP.

Possible models of packing for the crystals structure of iP(R,S)3MP have been found performing calculations of the packing energy of chains of the random copolymer having conformation as in Figure 8, for the space group  $P2_1/b$ . The chains of iP(R,S)3MP are characterized by disorder in the conformations of the side groups, which assume the different conformations of Table 3 shown in Figure 7, depending on the chirality of the monomeric unit and the handedness of the helix. The possible models of packing have been found simulating the chain of the random copolymer of Figure 8 with the limit conformations A, B, C of iP(S)3MP and D, E, F of iP(R)3MP of Figure 7. The packing energy has been calculated for six limit ordered models of packing of space group symmetry  $P2_1/b$  characterized by chains having the six different conformations of Figure 7. The six limit ordered models of packing are defined as the models of conformations of the chains of Figure 7 and Table 3.

Since the position of the chain axis inside the unit cell has been fixed at the fractional coordinates  $x/a = 0$ ,  $y/b = 0.25$ , coincident with the crystallographic  $2_1$  axis of the space group  $P2_1/b$ , the lattice energy has been calculated varying only the orientation of the chain around its axis (defined by the angle  $\omega$ ,

shown in Figure 9), and the  $z$  coordinate, which defines the relative heights of the chains in the unit cell. The axes of the

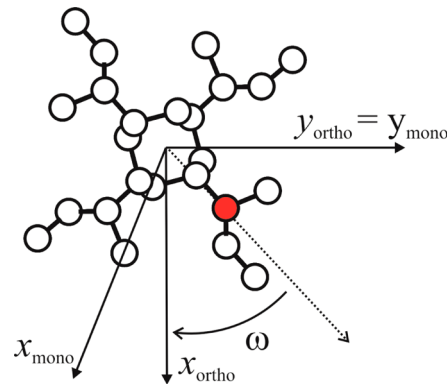


**Figure 9.** Definitions of the variables  $\omega$  and  $z$  used in the packing energy calculations in the orthogonal (ortho) and monoclinic (mono) coordinate systems. The value of  $\omega$  is positive for a clockwise rotation, and  $z$  is the height of the carbon atom indicated as a filled circle.

unit cell have been maintained constant at the experimental values  $a = 10.02 \text{ \AA}$ ,  $b = 18.48 \text{ \AA}$ ,  $c = 6.87 \text{ \AA}$ , and  $\gamma = 109.9^\circ$ .

Maps of the lattice energy for the six limit ordered models of packing of the six chains of Figure 7A-C,D-F as a function of  $\omega$  and  $z$  for the space group  $P2_1/b$  are reported in Figure 10. The maps are periodic over  $\omega = 180^\circ$  and  $z = c/2 = 3.43 \text{ \AA}$ ; therefore, only the regions with  $\omega = 0-180^\circ$  and  $z = 0-c/2 = 0-3.43 \text{ \AA}$  are shown.

The maps present one (Figure 10B,C,E,F) or two (Figure 10A,D) energy minima, which are periodically repeated after a

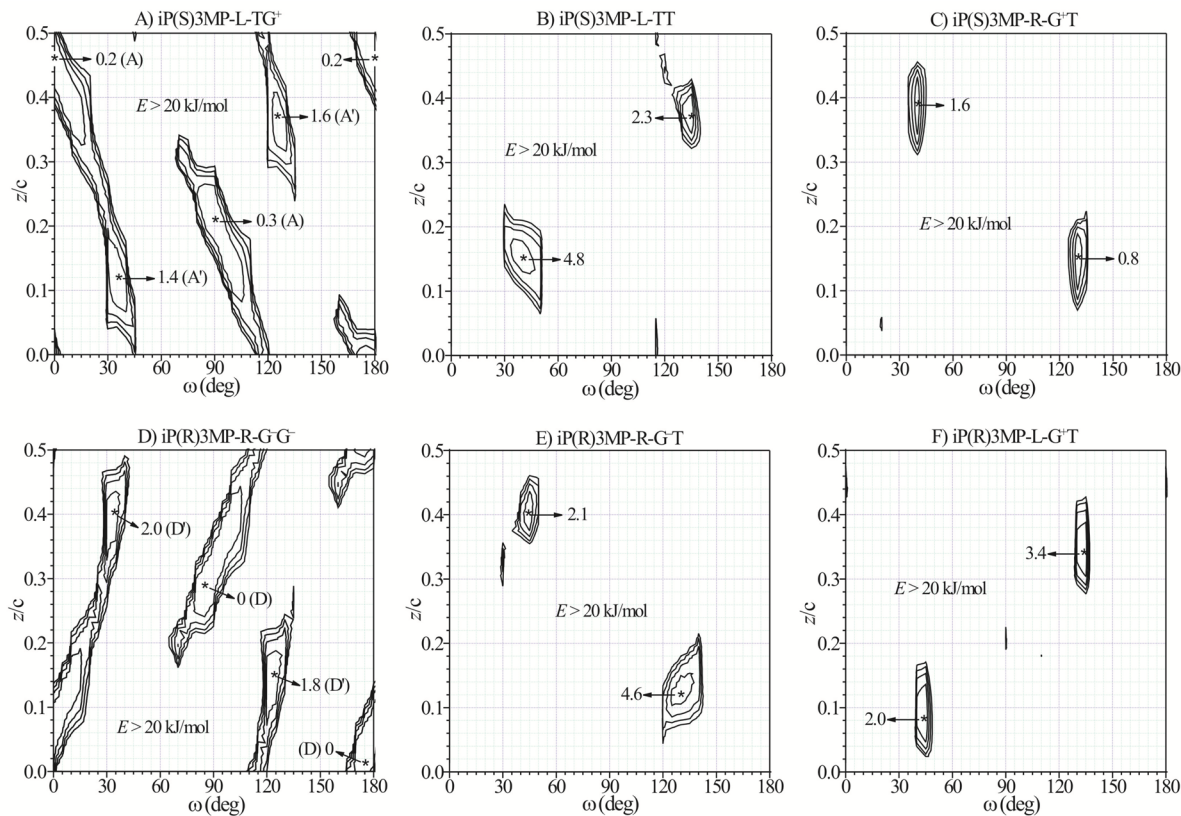


**Figure 10.** Maps of the packing energy as a function of  $\omega$  and  $z$  for the monoclinic unit cell with axes  $a = 10.02 \text{ \AA}$ ,  $b = 18.48 \text{ \AA}$ ,  $c = 6.87 \text{ \AA}$ , and  $\gamma = 109.9^\circ$ , for the space group symmetry  $P2_1/b$ , for the six limit ordered models of the chain conformation of iP(S)3MP or iP(R)3MP of Figure 7A–C,D–F and Table 3. In all models the chains have fixed 4/1 helical conformation and have their chain axes coincident with the crystallographic  $2_1$  helical axes of the unit cell in the space group  $P2_1/b$ . The curves are drawn at intervals of 5 kJ/(mol of monomeric unit) with respect to the absolute minimum of the maps assumed as zero in (D). The energy of the relative minima (\*) are also shown.

rotation of  $\omega = t = 90^\circ$ , where  $t$  is the unit twist of the 4/1 helix,  $t = 2\pi/4$ , and a translation of  $z = h = c/4 = 1.72 \text{ \AA}$ , where  $h$  is the unit height of the helix. The values of the energy minima and the corresponding values of  $\omega$  and  $z$  are reported in Table 4. It is apparent that equivalent absolute energy minima are obtained for the models iP(S)3MP-L-TG<sup>+</sup> (left-handed 4/1 chain of iP(S)3MP with  $\theta_3 = T$ ,  $\theta_4 = G^+$ ) (Figure 10A) and iP(R)3MP-R-G<sup>-</sup>G<sup>+</sup> (right-handed 4/1 chain of iP(R)3MP with  $\theta_3 = G^-$ ,  $\theta_4 = G^+$ ) (Figure 10D). Minima of slightly higher energy are obtained for the models iP(S)3MP-L-TT (left-handed 4/1 chain of iP(S)3MP with  $\theta_3 = T$ ,  $\theta_4 = T$ ) (Figure 10B) and iP(R)3MP-R-G<sup>-</sup>T (right-handed 4/1 chain of iP(R)3MP with  $\theta_3 = G^-$ ,  $\theta_4 = T$ ) (Figure 10E) and in the maps Figures 10C,F for the models iP(S)3MP-R-G<sup>+</sup>T (right-handed 4/1 chain of iP(S)3MP with  $\theta_3 = G^+$ ,  $\theta_4 = T$ ) and iP(R)3MP-L-G<sup>+</sup>T (left-handed 4/1 chain of iP(R)3MP with  $\theta_3 = G^+$ ,  $\theta_4 = T$ ), respectively. This indicates that the models A–F of Table 3 of the chains iP(S)3MP and iP(R)3MP (Figure 7A–F) are not only of low conformational energy but also of low packing energy in the space group  $P2_1/b$ . The data of Figure 10 and Table 4 also indicate that a high amount of conformational disorder may be included in the crystals due to the rotational freedom of the lateral groups defined by the values of the torsion angles  $\theta_3$  and  $\theta_4$  in S and R monomeric units of the copolymer iP(R,S)3MP, which can assume trans and gauche states at low cost of energy. The rotational freedom of the chains around the chain axis ( $\omega$ ) and the relative height of the chains along  $c$ , instead, are restricted around the minimum

energy of the maps, that is,  $\omega \approx 40 + n90^\circ$  and  $z/c \approx 0.1 + n0.25$ , and only for the models iP(S)3MP-L-TG<sup>+</sup> (left-handed 4/1 chain of iP(S)3MP with  $\theta_3 = T$ ,  $\theta_4 = G^+$ ) (Figure 10A) and iP(R)3MP-R-G<sup>-</sup>G<sup>+</sup> (right-handed 4/1 chain of iP(R)3MP with  $\theta_3 = G^-$ ,  $\theta_4 = G^+$ ) (Figure 10D) an additional minimum of packing energy occurs for  $\omega \approx 0$ . The rotational freedom of the chains around the chain axis ( $\omega$ ) and the relative height of the chains along  $c$ , depend, however, on the conformation of the side groups, in particular the torsion angle  $\theta_4$ . The comparison of the maps of Figure 10A,B and of the maps of Figure 10D,E shows that when the lateral groups assume conformation with  $\theta_4 = T$ , as in the models iP(S)3MP-L-TT of Figure 7B with  $\theta_3 = T$  and  $\theta_4 = T$ , and iP(R)3MP-R-G<sup>-</sup>T of Figure 7E with  $\theta_3 = G^-$  and  $\theta_4 = T$ , the space accessible for the packing of chains in the unit cell is more restricted and the energy minima of the maps of Figure 10B,E are narrower compared to those of the maps of Figure 10A,D of models of chains iP(S)3MP-L-TG<sup>+</sup> of Figure 7A and iP(R)3MP-R-G<sup>-</sup>G<sup>+</sup> of Figure 7D with  $\theta_4 = G^+$  and  $G^-$ , respectively. This indicates that even though the models of chains iP(S)3MP-L-TG<sup>+</sup> (Figure 7A) and iP(S)3MP-L-TT (Figure 7B), corresponding to the two possible values of  $\theta_4 = G^+$  or  $T$ , are conformationally isoenergetic, the packing of the chain iP(S)3MP-L-TG<sup>+</sup> is more favorable in term of accessible space. Analogously, even though the models of chains iP(R)3MP-R-G<sup>-</sup>G<sup>+</sup> (Figure 7D) and iP(R)3MP-R-G<sup>-</sup>T (Figure 7E), corresponding to the two possible values of  $\theta_4 = G^-$  or  $T$ , have the same conformational energy, the packing of the chain iP(R)3MP-L-G<sup>-</sup>G<sup>+</sup> is more favorable. This possibly

**Table 4.** Values of the Packing Energy Minima and Corresponding Values of  $\omega$  and  $z$  Found in the Maps of the Packing Energy of **Figure 10** for the Chain Models iP(S)3MP-L-TG<sup>+</sup> (left-handed 4/1 Chain of iP(S)3MP with  $\theta_3 = T$ ,  $\theta_4 = G^+$ ) (**Figure 10A**), iP(S)3MP-L-TT (Left-Handed 4/1 Chain of iP(S)3MP with  $\theta_3 = T$ ,  $\theta_4 = T$ ) (**Figure 10B**), iP(S)3MP-R-G<sup>+</sup>T (Right-Handed 4/1 Chain of iP(S)3MP with  $\theta_3 = G^+$ ,  $\theta_4 = T$ ) (**Figure 10C**), iP(R)3MP-R-G<sup>-</sup>G<sup>-</sup> (Right-Handed 4/1 Chain of iP(R)3MP with  $\theta_3 = G^-$ ,  $\theta_4 = G^-$ ) (**Figure 10D**), iP(R)3MP-R-G<sup>-</sup>T (Right-Handed 4/1 Chain of iP(R)3MP with  $\theta_3 = G^-$ ,  $\theta_4 = T$ ) (**Figure 10E**) and iP(R)3MP-L-G<sup>+</sup>T (Left-Handed 4/1 Chain of iP(R)3MP with  $\theta_3 = G^+$ ,  $\theta_4 = T$ ) (**Figure 10F**)<sup>a</sup>

model of packing	model of chain	$\theta_1$ (deg)	$\theta_2$ (deg)	$\theta_3$ (deg)	$\theta_4$ (deg)	$\omega$ (deg)	$z/c$	$E_{\text{pack}}^{\text{a}}$ (kJ/mol mu)	minima of maps of <b>Figure 10</b>
iP(S)3MP									
A	iP(S)3MP-L-TG <sup>+</sup> (down)	80	-160	-160	70	0	0.46	0.2	A
						90	0.21	0.3	
A'	iP(S)3MP-L-TG <sup>+</sup> (down)	80	-160	-160	70	35	0.12	1.4	A'
						125	0.37	1.6	
B	iP(S)3MP-L-TT (down)	80	-160	-160	170	40	0.15	4.8	B
						135	0.37	2.3	
C	iP(S)3MP-R-G <sup>+</sup> T (up)	150	-80	50	170	40	0.39	1.6	C
						130	0.15	0.8	
iP(R)3MP									
D	iP(R)3MP-R-G <sup>-</sup> G <sup>-</sup> (up)	160	-80	-80	-70	-5	0.042	0	D
						85	0.29	0	
D'	iP(R)3MP-R-G <sup>-</sup> G <sup>-</sup> (up)	160	-80	-80	-70	35	0.40	2.0	D'
						125	0.15	1.8	
E	iP(R)3MP-R-G <sup>-</sup> T (up)	160	-80	-70	-160	45	0.40	2.1	E
						130	0.12	4.6	
F	iP(R)3MP-L-G <sup>+</sup> T (down)	80	-150	80	-160	45	0.08	2.0	F
						135	0.35	3.4	

<sup>a</sup>The values of the packing energy  $E_{\text{pack}}$  correspond to the minima of the maps of **Figure 10** at  $\omega$  and  $z/c$ , and  $\omega + 90^\circ$  and  $z/c + 0.25$  and are scaled with respect to the absolute minimum of the maps of **Figure 10** assumed as zero.

indicates that the hypothesized disorder in the conformation of the lateral groups, due to the two possible values assumed by  $\theta_4$  in both S and R monomeric units of the copolymer iP(*R,S*)3MP in the unit cell is not completely statistical.

The six limit ordered models of packing A–C and D–F of **Table 4**, corresponding to the energy minima in the maps of **Figure 10**, are shown in **Figure 11**. Since the models C and F have identical azimuthal settings of chains (angle  $\omega$ ), also the projections in the *ab* plane are identical (**Figure 11C,F**), provided that the chains are anticlined (up and down), as for the models C, iP(S)3MP-R-G<sup>+</sup>T (up), and F, iP(R)3MP-L-G<sup>+</sup>T (down). Also, the models B, iP(S)3MP-L-TT (down), and E, iP(R)3MP-R-G<sup>-</sup>T (up), have identical azimuthal setting and the chains are anticlined, so that the projections in the *ab* plane are identical (**Figure 11B,E**).

Calculations of structure factors have been performed for the six limit ordered models of packing of **Figure 11** and **Table 4** corresponding to the energy minima of the maps of **Figure 10**. A comparison between observed structure factors ( $F_0$ ), evaluated from the X-ray powder diffraction profile of **Figure 1b** and the fiber diffraction pattern of **Figure 3**, and structure factors calculated ( $F_c$ ) for the six limit ordered models A–F of **Figure 11** for the space group  $P2_1/b$  is reported in **Tables 5** and **6**, respectively (more complete lists of calculated structure factors are reported as *Supporting Information*). A direct comparison between the experimental X-ray powder diffraction profile of **Figure 1b**, after the subtraction of the amorphous halo, and the calculated profiles for the six limit ordered models of **Figure 11** is reported in the **Figure 12**, whereas the calculated X-ray fiber diffraction patterns to compare with the experimental pattern of **Figure 3** are shown in **Figure 13** (see *Supporting Information* for details of structure factors calculations).

It is worth noting that the diffraction profiles calculated for the models of packing A (profile b of **Figure 12A**), B (profile c of **Figure 12A**), and C (profile d of **Figure 12A**) of **Figure 11** are identical to those of the models D, E, and F respectively. A not completely satisfactory agreement between calculated structure factors and experimental intensities observed in the X-ray powder profile of **Figure 1b** and X-ray fiber diffraction pattern of **Figure 3** has been obtained for all the limit ordered models of **Table 4** and **Figure 11**. The calculated diffraction profiles for every model of **Figure 11** present basically the most important features of the experimental diffraction pattern, but with different defects. In particular, the powder and fiber diffraction patterns calculated for the models A and D of **Figure 11A,D** present a too low intensity of the 020 reflection at  $2\theta = 10.18^\circ$  and of the 021 reflection on the first layer line at  $2\theta = 16.45^\circ$  (**Tables 5** and **6**, profile b of **Figure 12A** and pattern B of **Figure 13**), compared to the experimental intensities (profile a of **Figure 12A** and **Figure 13A**). The diffraction patterns calculated for the models B and E of **Figure 11B,E** present a too low intensity of the 020 reflection at  $2\theta = 10.18^\circ$  and too high intensities of the  $\bar{1}\bar{2}0$  reflection at  $2\theta = 11.26^\circ$  and of  $\bar{1}\bar{1}1$ , 101, and 021 reflections on the first layer line at  $2\theta = 15.75^\circ$ ,  $16.96^\circ$ , and  $16.45^\circ$ , respectively (**Table 5** and **6** and profile c of **Figure 12A** and pattern C of **Figure 13**). The diffraction patterns calculated for the models C and F of **Figure 11C,F** present almost right intensities of the equatorial 100 and 020 reflections at  $2\theta = 9.39^\circ$  and  $10.18^\circ$ , respectively, and of  $\bar{1}\bar{1}1$ , 101, and 021 reflections on the first layer line at  $2\theta = 15.75^\circ$ ,  $16.96^\circ$ , and  $16.45^\circ$ , respectively, but present a too high intensity of the 011 reflection at  $2\theta = 13.86^\circ$  (**Tables 5** and **6** and profile d of **Figure 12A** and pattern D of **Figure 13**), which is absent in the experimental powder and fiber diffraction patterns.

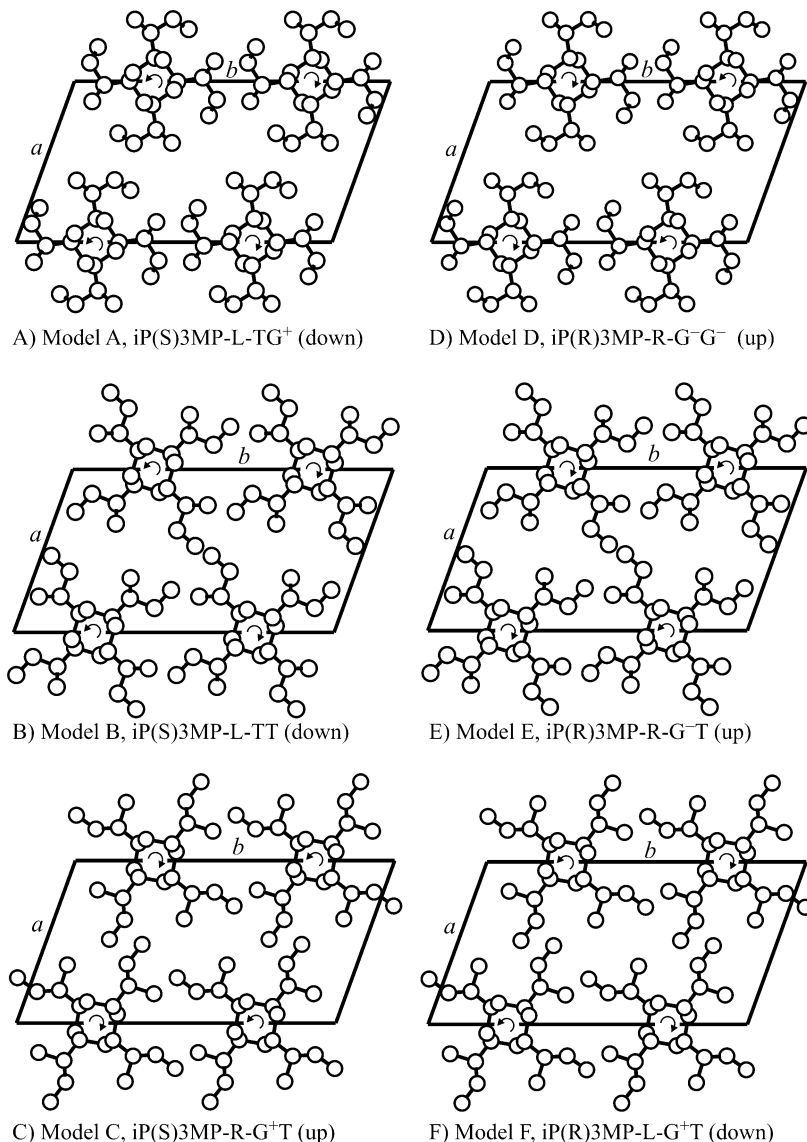


**Figure 11.** Limit ordered models of packing of chains of *iP(S)3MP* (A–C) or *iP(R)3MP* (D–F) in the monoclinic unit cell with axes  $a = 10.02 \text{ \AA}$ ,  $b = 18.48 \text{ \AA}$ ,  $c = 6.87 \text{ \AA}$ , and  $\gamma = 109.9^\circ$  according to the space group  $P2_1/b$ , corresponding to the minima of the maps of packing energy of Figure 10 and Table 4.

The packing models of the pure enantiomers *iP(R)3MP* and *iP(S)3MP* of Figure 11 represent only limit ordered models of the structure of the random copolymer *iP(R,S)3MP*. The structure of the real crystalline modification of *iP(R,S)3MP* is obviously disordered due to configurational disorder in the sequence of R and S monomeric units along the chains of crystallizable stretches, as in the disordered models of chains of Figure 8, conformational disorder of the lateral groups, and also to the presence of structural disorder in the packing of chains. This disorder has been modeled and limit disordered models of packing have been obtained by assuming that each site of the crystalline lattice with space group symmetry  $P2_1/b$  may be occupied with different probabilities by the different chains of Figure 7, having different chirality of the side groups, different handedness of the helical conformation, different up/down orientations, and different conformations of the lateral groups. Several possibilities have been considered. For limit disordered models made by a statistical occupancy on the lattice sites of helices of identical handedness but different chirality of monomeric unit and conformations of the lateral groups, the

agreement between experimental and calculated diffracted intensities obtained for the limit ordered models of pure enantiomers of Figure 11 could not be improved.

A remarkable improvement of the agreement was obtained for limit disordered models characterized by disorder in the random substitution in the sites of the lattice of chains having opposite helical handedness and opposite chirality of the lateral groups, as in the model of Figure 14. In this model each site of the lattice is occupied with the same probability by chains *iP(S)3MP-R-G<sup>+</sup>T* (up) (Figure 7C) and *iP(R)3MP-L-G<sup>+</sup>T* (down) (Figure 7F), having opposite chirality in the helical hand (right-handed and left-handed), opposite S and R chirality of the lateral groups, and opposite up and down orientation (anticlined chains). As shown in the limit ordered models of Figure 11C,F, built with these two models of chains, the chains *iP(S)3MP-R-G<sup>+</sup>T* (up) and *iP(R)3MP-L-G<sup>+</sup>T* (down) have not only identical projections in the  $ab$  plane (Figure 14A), but also similar outside envelope for the lateral side groups as shown in Figure 14B. The structure factors calculated for the limit disordered model of Figure 14 are reported in Tables 5 and 6,

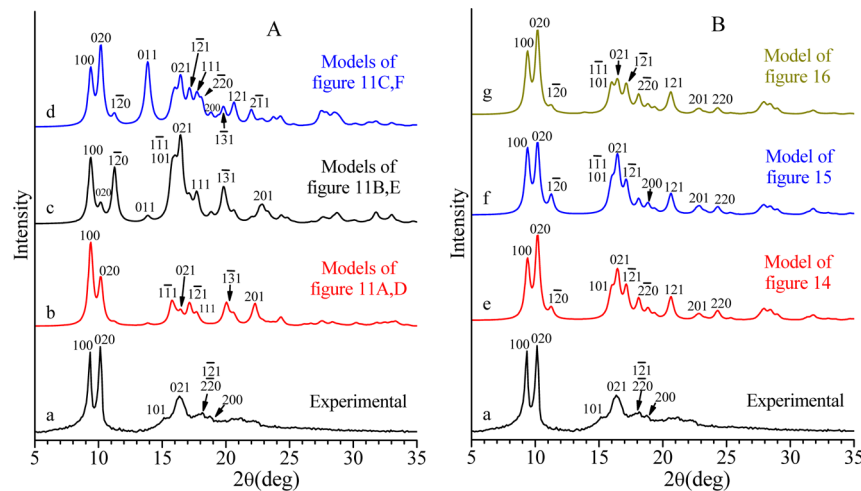


**Figure 12.** Comparison between the experimental X-ray powder diffraction profile of iP(R,S)3MP of Figure 1b after subtraction of the amorphous halo (a) and diffraction profiles calculated for the limit ordered models of packing of space group symmetry  $P_{2_1}/b$  of Figures 11A,D (b), 11B,E (c), and 11C,F (d), for the limit disordered models of Figures 14 (e) and 15 (f) and for the limit disordered model of packing of space group symmetry  $P_{2_1}$  of Figure 16 (g).

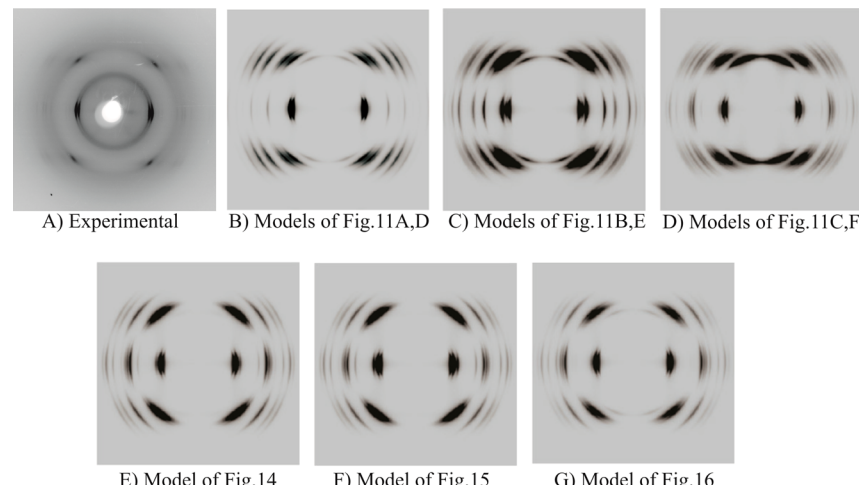


**Figure 13.** Comparison between the experimental X-ray fiber diffraction pattern of iP(R,S)3MP (A) and diffraction patterns calculated for the limit ordered models of packing of space group symmetry  $P_{2_1}/b$  of Figures 11A,D (B), 11B,E (C), and 11C,F (D), for the limit disordered models of Figures 14 (E) and 15 (F) and for the limit disordered model of packing of space group symmetry  $P_{2_1}$  of Figure 16 (G).

whereas the calculated powder diffraction profile is reported in Figure 12B (profile e) and the calculated fiber diffraction pattern is shown in Figure 13E. A very good agreement between observed and calculated diffraction profiles is obtained. According to the experimental diffraction pattern, in the calculated diffraction profile e of Figure 12B the 011 reflection at  $2\theta = 13.86^\circ$  is absent, the intensity of the  $\bar{1}\bar{2}0$  reflection at  $2\theta = 11.26^\circ$  is very low, and the intensity ratios of first layer lines and equatorial reflections in the range of  $2\theta = 15^\circ - 21^\circ$ , in particular the 101, 021,  $\bar{1}\bar{2}1$ ,  $\bar{2}\bar{2}0$ , and 121 reflections at  $2\theta = 15.96^\circ$ ,  $16.45^\circ$ ,  $17.14^\circ$ ,  $18.11^\circ$ , and  $20.64^\circ$ , respectively, are similar to those in the experimental profile. The disagreement factor calculated for both observed and nonobserved reflections is 15%. The diffraction data and the agreement indicates that in the crystals of iP(R,S)3MP *chain stretches of sequences of monomeric units with prevailing S configuration tend to assume a right-handed helical conformation, whereas those of prevailing R configuration tend to assume a left-handed helical conformation*. The prevailing combinations of (S/R)chirality-(Right/Left)-helical chirality are therefore S-right, R-left, as in chain models

C, iP(S)3MP-R-G<sup>+</sup>T (up) (Figure 7C) and F, iP(R)3MP-L-G<sup>+</sup>T (down) (Figure 7F). Disorder originates from the random substitution of helical stretches of opposite R and S configuration and helical handedness provided that they are also anticlined, that is, one up and the other down.

In this model the possible disorder in the conformation of the lateral groups is not present and both S and R monomeric units are characterized by conformation of the side groups with  $\theta_3 = G^+$  and  $\theta_4 = T$ , as in the ordered models C and F of the pure enantiomers of Figure 11C,F. This conformation is characterized by the ethyl groups in a double-gauche arrangement to both CH<sub>2</sub> groups of the backbone (Figure 8A',B'). Therefore, even though the conformation of the side groups with  $\theta_4 = G^+$  or  $G^-$  is slightly favored in term of packing energy (Figure 10A,D), the diffraction agreement indicates prevalence of the conformation of the lateral groups with  $\theta_4 = T$ .

In spite of the good agreement already achieved for the model of Figure 14, some kind of conformational disorder should be also included in the crystals. Moreover, even though

**Table 5. Comparison between Observed Structure Factors  $F_o = (I/LP)^{1/2}$ , Evaluated from the Intensities  $I$  Observed in the X-ray Powder Diffraction Profile of iP(R,S)3MP of Figure 1b, and Calculated Structure Factors,  $F_c = (\sum |F_i|^2 M_i)^{1/2}$ , for the Limit Ordered Models of Packing of Figure 11 of the Pure Enantiomers iP(S)3MP and iP(R)3MP and the Limit Disordered Models of Packing of Figures 14 and 15 of the Random Copolymer iP(R,S)3MP in the Monoclinic Unit Cell with Axes  $a = 10.02 \text{ \AA}$ ,  $b = 18.48 \text{ \AA}$ ,  $c = 6.87 \text{ \AA}$ , and  $\gamma = 109.9^\circ$  According to the Space Group  $P2_1/b^a$**

$hkl$	$2\theta_o$ (deg)	$2\theta_c$ (deg)	$d_o$ (\text{\AA})	$d_c$ (\text{\AA})	$F_o = (I_o/LP)^{1/2}$	$F_c = (\sum  F_i ^2 M_i)^{1/2}$				
						Models of Figure 11A,D	Model of Figures 11B,E	Models of Figure 11C,F	Model of Figure 14	Model of Figure 15
100	9.34	9.39	9.47	9.42	87	138	93	84	84	85
020	10.19	10.18	8.68	8.69	91	110	48	109	109	96
120	—	11.26	—	7.86	—	26	102	42	42	54
011	—	13.86	—	6.39	—	35	44	142	—	—
{111}	15.14	15.75	5.62	89	122 25 58	122 79 80	58 94 24	— 94 24	— 97 35	— 91 35
		15.96	5.85							
		16.06	5.55							
021	16.36	16.45	5.41	5.39	142	88	178	130	130	139
{121}	18.16	17.14	5.17	117	125 93 13	82 111 3	110 106 89	110 176 89	110 141 70	104 126 70
		17.72	4.88							
		18.11	4.90							
{200}	18.74	18.84	4.71	109	19 13	58 23	62	64 44	78	63 40
		19.37	4.58							
{131}	21.17	19.81	4.48	143	55 144 50 93	132 64 12 174	93 2 26 113	— — 26 113	— — 116 105	— — 18 107
		20.05	4.43							
		20.44	4.34							
		20.64	4.30							
{211}	22.13	22.00	4.04	116	54 158 21 58 48 50 41 97 26	50 17 75 98 72 29 6 56 44	101 9 38 58 25 73 64 — 55	— 9 38 58 25 — 63 — 55	— 10 45 66 112 — 52 — 53	— 10 45 66 112 — 52 — 53
		22.29	3.99							
		22.63	3.93							
		22.89	3.88							
		23.33	4.02							
		23.73	3.75							
		24.24	3.67							
		24.33	3.66							
		24.37	3.65							
211	—	24.85	—	3.58	—	5	58	5	—	—
140	—	25.33	—	3.52	—	9	24	36	36	34
002	—	25.94	—	3.43	—	6	4	6	6	6
241	—	26.13	—	3.41	—	44	11	11	11	7
012	—	26.45	—	3.37	—	30	4	20	—	—
320	—	26.70	—	3.34	—	52	33	10	10	15
151	—	27.41	—	3.25	—	47	23	77	—	—
112	—	27.52	—	3.24	—	54	40	71	—	—
102	—	27.64	—	3.23	—	56	55	54	54	54
221	—	27.66	—	3.22	—	33	25	9	9	12
022	—	27.93	—	3.19	—	18	45	93	93	83
122	—	28.36	—	3.15	—	72	22	42	42	29
300	—	28.42	—	3.14	—	27	48	52	52	52
141	—	28.52	—	3.13	—	11	8	58	58	49
112	—	28.72	—	3.11	—	26	87	80	—	—
051	—	28.79	—	3.10	—	22	41	30	—	—
340	—	28.86	—	3.09	—	32	3	5	5	4
160	—	29.01	—	3.08	—	17	45	61	61	58
251	—	29.28	—	3.05	—	32	13	8	—	—
321	—	29.75	—	3.00	—	21	32	15	15	18

<sup>a</sup>The experimental Bragg angles ( $2\theta_o$ ) and Bragg distances ( $d_o$ ) observed in the X-ray powder diffraction profile of iP(R,S)3MP of Figure 1b and those calculated ( $2\theta_c$  and  $d_c$ ) for the monoclinic unit cell with axes  $a = 10.02 \text{ \AA}$ ,  $b = 18.48 \text{ \AA}$ ,  $c = 6.87 \text{ \AA}$ , and  $\gamma = 109.9^\circ$  are also reported.

the diffraction data indicate that in the chains of the random copolymer iP(R,S)3MP the prevailing combinations of (S/R) chirality-(Right/Left)helical chirality are S-right, R-left, disorder in this combination may be present and sequences of S monomeric units may also assume left-handed helical conformation and sequences of R monomeric units may also assume right-handed helical conformation, as in the models of

chains of Figures 7B,C' and 7E,F', corresponding to the combinations S-left and R-right.

Disorder in the succession of R and S monomeric units along the chain of iP(R,S)3MP, conformational disorder of the side groups, disorder in the helical chirality and in the up-down orientation of the chains can be modeled by assuming that each site of the crystalline lattice is occupied with a given probability

**Table 6.** Comparison between Observed Structure Factors  $F_o = (I/LP)^{1/2}$ , Evaluated from the Intensities  $I$  Observed in the X-ray Fiber Diffraction Pattern of iP(R,S)3MP of Figure 3, and Calculated Structure Factors,  $F_c = (\sum |F_i|^2 M_i)^{1/2}$ , for the Limit Ordered Models of Packing of Figure 11 of the Pure Enantiomers iP(S)3MP and iP(R)3MP and the Limit Disordered Models of Packing of Figures 14 and 15 of the Random Copolymer iP(R,S)3MP in the Monoclinic Unit Cell with Axes  $a = 10.02 \text{ \AA}$ ,  $b = 18.48 \text{ \AA}$ ,  $c = 6.87 \text{ \AA}$ , and  $\gamma = 109.9^\circ$  According to the Space Group  $P2_1/b$ <sup>a</sup>

$hkl$	$2\theta_o$ (deg)	$2\theta_c$ (deg)	$d_o$ ( $\text{\AA}$ )	$d_c$ ( $\text{\AA}$ )	$F_o = (I_o/LP)^{1/2}$	$F_c = (\sum  F_i ^2 M_i)^{1/2}$				
						Models of Figure 11A,D	Models of Figure 11B,E	Models of Figure 11C,F	Model of Figure 14	Model of Figure 15
100	9.38	9.39	9.43	9.42	79	98	66	59	59	60
020	10.18	10.18	8.69	8.69	100	78	34	77	77	68
1̄20	11.75	11.26	7.53	7.86	26	18	72	29	29	38
110	12.80	12.11	6.91	7.30	24	—	—	—	—	—
120	16.78	16.06	5.28	5.52	31	41	56	17	17	25
220	18.14	18.11	4.89	4.90	23	10	2	63	63	50
{200 1̄40}	18.86 19.37	4.7 4.58	4.71 4.58	44	13 9 16 16	41 44	45 55 31 31	45 55 31 31	44 52 28	44 52
{040 240}	20.47 22.63	4.34 3.93	4.34 3.93	33	35 15 39	9 53 54	18 27 32	18 27 32	13 35 32	13 35 32
{220 140}	25.29 25.33	3.52 3.52	3.65 3.52	23	18 6 19 19	31 17 36	39 25 47	39 25 47	37 44 24	37 44 24
3̄20	26.28	26.70	3.39	3.34	10	36	23	7	7	10
300	—	28.42	—	3.14	—	19	34	37	37	36
3̄40	—	28.86	—	3.09	—	23	2	4	4	3
1̄60	—	29.01	—	3.08	—	12	32	43	44	41
2̄60	—	30.23	—	2.96	—	39	7	9	9	9
060	—	30.88	—	2.90	—	8	8	—	—	2
240	—	32.44	—	2.76	—	41	12	6	6	7
320	—	33.48	—	2.68	—	23	8	11	11	7
3̄60	—	34.23	—	2.62	—	34	2	12	12	9
011	—	13.86	—	6.39	—	17	22	71	—	—
{1̄11 101}	15.55	5.7	5.62	46	61 12 62	61 39 73	29 47 55	— 47 47	— 45 45	— 45 45
021	16.55	16.45	5.34	5.39	71	44	89	65	65	70
{1̄21 111 1̄31 031}	18.30	4.85	5.17 5.00 4.48 4.43	52	62 42 27 72	41 56 101 32	55 53 89 —	55 — 55 —	52 — 52 —	52 — 52 —
121	21.15	20.64	4.20	4.30	35	47	37	56	56	53
{211 221 201 1̄41 2̄31 041 131 211 241}	22.00	4.03	4.04 3.99 3.88 3.81 3.75 3.67 3.66 3.58 3.41	51	27 79 29 24 111 20 46 3 22	25 8 49 36 14 3 28 29 5	51 4 29 12 79 32 — 2 6	— 4 29 12 — 32 — — 6	— 5 33 17 — 26 — — 3	— 5 33 17 — 26 — — 3
1̄51	—	27.41	—	3.25	—	24	11	38	—	—
221	—	27.66	—	3.22	—	17	12	4	4	6
141	—	28.52	—	3.13	—	5	4	29	29	24
051	—	28.79	—	3.10	—	11	20	15	—	—
2̄51	—	29.28	—	3.05	—	16	6	4	—	—
321	—	29.75	—	3.00	—	11	16	7	7	9
002	—	25.94	—	3.43	—	4	3	6	5	4
012	—	26.45	—	3.37	—	15	2	10	—	—
1̄12	—	26.52	—	3.24	—	27	20	36	—	—
102	—	27.64	—	3.23	—	28	27	27	27	27
022	—	27.93	—	3.19	—	9	23	46	46	42

<sup>a</sup>The experimental Bragg angles ( $2\theta_o$ ) and Bragg distances ( $d_o$ ) observed in the X-ray fiber diffraction pattern of iP(R,S)3MP of Figure 3 and those calculated ( $2\theta_c$  and  $d_c$ ) for the monoclinic unit cell with axes  $a = 10.02 \text{ \AA}$ ,  $b = 18.48 \text{ \AA}$ ,  $c = 6.87 \text{ \AA}$  and  $\gamma = 109.9^\circ$  are also reported.

by chains iP(S)3MP-R-G<sup>+</sup>T (up) (Figure 7C), iP(R)3MP-L-G<sup>+</sup>T (down) (Figure 7F), iP(S)3MP-L-TT (down) (Figure 7B), and iP(R)3MP-R-G<sup>-</sup>T (up) (Figure 7E). The chain models C, iP(S)3MP-R-G<sup>+</sup>T (up), and E, iP(R)3MP-R-G<sup>-</sup>T (up), are isochemical (up) and isomorphous (right-handed) but

have opposite S and R chirality of the lateral groups, with chirality combinations (S)-right-handed and (R)-right-handed, and different conformations of the side groups with  $\theta_3 = G^+$  or  $G^-$ . Analogously, the chain models F, iP(R)3MP-L-G<sup>+</sup>T (down), and B, iP(S)3MP-L-TT (down), are isochemical

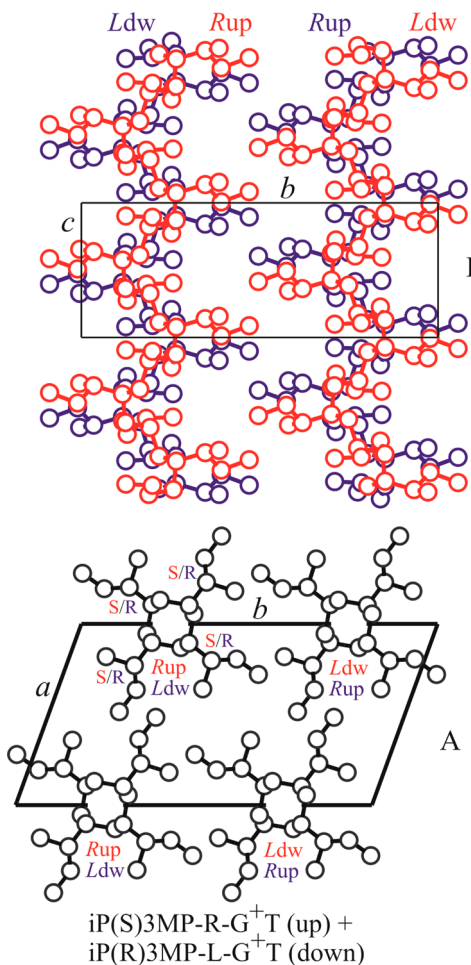


**Figure 14.** Limit disordered model of packing of *iP(R,S)3MP* in the monoclinic unit cell with axes  $a = 10.02 \text{ \AA}$ ,  $b = 18.48 \text{ \AA}$ ,  $c = 6.87 \text{ \AA}$ , and  $\gamma = 109.9^\circ$  according to the space group  $P2_1/b$  viewed in  $ab$  (A) and  $bc$  (B) projections. The crystalline lattice at  $x = 0$  and  $y = 0.25$  is occupied with the same probability by chains *iP(S)3MP-R-G<sup>+</sup>T* (up) (chain model of Figure 7C) and *iP(R)3MP-L-G<sup>+</sup>T* (down) (chain model of Figure 7F), having opposite chirality in the helical hand (right-handed and left-handed), opposite S and R chirality of the lateral groups, and opposite up and down orientation (anticlined chains). The chains *iP(S)3MP-R-G<sup>+</sup>T* (up) and *iP(R)3MP-L-G<sup>+</sup>T* (down) have identical projections in the  $ab$  plane (A) and similar outside envelope for the lateral side groups (B). *Rup* and *Ldw* indicate right-handed helix with up orientation and left-handed helix with down orientation, whereas *S/R* indicates the chirality of the methine carbons of the lateral groups.

(down) and isomorphous (left-handed) but have opposite S and R chirality of the lateral groups, with combinations (R)-left-handed and (S)-left-handed, and different conformations of the side groups with  $\theta_3 = G^+$  or T. This limit disordered model for the structure of *iP(R,S)3MP* is shown in Figure 15. In this limit disordered model, the substitution type disorder of enantiomorphous, right- and left-handed, and anticlined chains of opposite S and R chirality of the side groups of the model of Figure 14 is coupled with conformational disorder of the side groups and different combinations (*S/R*)chirality-(Right/Left)-helical chirality. The degrees of different types of disorder are defined by the occupancy factors of atoms belonging to the different model chains. The occupancy factors of all atoms of the right-handed up chains are  $p/2$  for *iP(S)3MP-R-G<sup>+</sup>T* (up) (chain model C) and  $(1 - p)/2$  for *iP(R)3MP-R-G<sup>-</sup>T* (up) (chain model E), and the occupation factors of atoms of the left

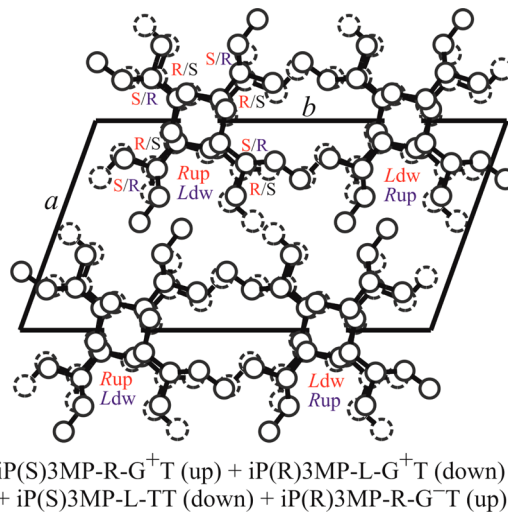


**Figure 15.** Limit disordered model of packing of *iP(R,S)3MP* in the monoclinic unit cell with axes  $a = 10.02 \text{ \AA}$ ,  $b = 18.48 \text{ \AA}$ ,  $c = 6.87 \text{ \AA}$ , and  $\gamma = 109.9^\circ$  according to the space group  $P2_1/b$ . The crystalline lattice at  $x = 0$  and  $y = 0.25$  is occupied with the same probability by chains *iP(S)3MP-R-G<sup>+</sup>T* (up) (chain model of Figure 7C), *iP(R)3MP-L-G<sup>+</sup>T* (down) (chain model of Figure 7F), *iP(S)3MP-L-TT* (down) (chain model of Figure 7B), and *iP(R)3MP-R-G<sup>-</sup>T* (up) (chain model of Figure 7E), having opposite chirality in the helical hand (right-handed and left-handed), opposite S and R chirality of the lateral groups, opposite up and down orientation (anticlined chains) and different combinations (*S/R*)chirality-(Right/Left)-helical chirality. *Rup* and *Ldw* indicate right-handed helix with up orientation and left-handed helix with down orientation, whereas *S/R* indicates the chirality of the methine carbons of the lateral groups.

handed down chains are  $p/2$  for *iP(R)3MP-L-G<sup>+</sup>T* (down) (chain model F) and  $(1 - p)/2$  for *iP(S)3MP-L-TT* (down) (chain model B). A value of the parameter  $p = 1$  would correspond to the model of Figure 14, including substitution type disorder of enantiomorphous and anticlined chains of opposite S and R chirality, and no conformational disorder. The case  $0.5 < p < 1$  corresponds to the presence of stretches of left-(right-) handed 4/1 helices of a prevailing R (S) configuration, including  $(1 - p)/2$  stretches of left- (right-) handed 4/1 helices of a prevailing S (R) configuration and different conformation of the lateral groups, disorder in the right/left-handed helices substitution being still present. The structure factors calculated for the limit disordered model of Figure 15 for the space group  $P2_1/b$  for  $p = 0.8$  are reported in Table 5 (for powder diffraction) and Table 6 (for fiber diffraction) (see Supporting Information for more complete lists of calculated structure factors). The calculated diffraction profile for the model of Figure 15 is reported in Figure 12B (profile f) in comparison with the experimental X-ray powder diffraction profile, whereas the calculated fiber diffraction pattern is shown in Figure 13F. A good agreement between calculated and observed structure factors is obtained for the ideal limit disordered model of Figure 15 in all cases. In particular, for  $p = 0.8$  the agreement is slightly improved compared to that of the model of Figure 14 with a value of the disagreement factor  $R$  of 14%. The fractional coordinates of carbon atoms of the asymmetric units of the model of Figure 15 are reported in Table 7.

Inspection of the X-ray fiber diffraction data of Figure 3 and Table 1 shows the presence of a very weak reflection on the equator at  $2\theta = 12.8^\circ$ , indexed as 110 reflection that is absent in

**Table 7.** Fractional Coordinates of the Carbon Atoms of the Asymmetric Unit (Two Monomeric Units) of the Model of Figure 15 for the Crystal Structure of iP(R/S)3MP in the Monoclinic Unit Cell with Axes  $a = 10.02 \text{ \AA}$ ,  $b = 18.48 \text{ \AA}$ ,  $c = 6.87 \text{ \AA}$ , and  $\gamma = 109.9^\circ$  According to the Space Group  $P2_1/b^a$

atom	$x/a$	$y/b$	$z/c$	occupancy factor
C <sub>1</sub>	-0.106	0.178	0.463	0.4
C <sub>2</sub>	-0.203	0.097	0.394	0.4
C <sub>3</sub>	-0.194	0.028	0.514	0.4
C <sub>4</sub>	-0.279	-0.048	0.417	0.4
C <sub>5</sub>	-0.358	0.093	0.386	0.4
C <sub>6</sub>	0.131	0.303	0.177	0.4
C <sub>7</sub>	0.103	0.216	0.214	0.4
C <sub>8</sub>	0.054	0.194	0.427	0.4
C <sub>9</sub>	0.230	0.191	0.151	0.4
C <sub>10</sub>	0.363	0.221	0.280	0.4
C <sub>11</sub>	0.485	0.196	0.204	0.4
C <sub>12</sub>	0.181	0.103	0.133	0.4
C <sub>1'</sub>	-0.054	0.306	0.573	0.4
C <sub>2'</sub>	-0.103	0.284	0.786	0.4
C <sub>3'</sub>	-0.131	0.197	0.823	0.4
C <sub>4'</sub>	-0.230	0.309	0.849	0.4
C <sub>5'</sub>	-0.363	0.279	0.719	0.4
C <sub>6'</sub>	-0.485	0.304	0.796	0.4
C <sub>7'</sub>	-0.181	0.397	0.866	0.4
C <sub>8'</sub>	-0.106	0.178	0.037	0.4
C <sub>9'</sub>	-0.203	0.097	0.105	0.4
C <sub>10'</sub>	-0.194	0.028	-0.014	0.4
C <sub>11'</sub>	-0.279	-0.048	0.083	0.4
C <sub>12'</sub>	-0.358	0.093	0.114	0.4
C <sub>1''</sub>	0.116	0.316	0.548	0.1
C <sub>2''</sub>	0.221	0.394	0.620	0.1
C <sub>3''</sub>	0.374	0.395	0.648	0.1
C <sub>4''</sub>	0.470	0.469	0.746	0.1
C <sub>5''</sub>	0.220	0.462	0.489	0.1
C <sub>6''</sub>	0.040	0.190	0.081	0.1
C <sub>7''</sub>	0.092	0.209	0.294	0.1
C <sub>8''</sub>	0.139	0.297	0.333	0.1
C <sub>9''</sub>	0.209	0.176	0.354	0.1
C <sub>10''</sub>	0.150	0.088	0.392	0.1
C <sub>11''</sub>	0.261	0.058	0.477	0.1
C <sub>12''</sub>	0.333	0.196	0.208	0.1
C <sub>1'''</sub>	0.116	0.316	0.952	0.1
C <sub>2'''</sub>	0.139	0.297	0.167	0.1
C <sub>3'''</sub>	0.221	0.394	0.880	0.1
C <sub>4'''</sub>	0.374	0.395	0.851	0.1
C <sub>5'''</sub>	0.470	0.469	0.754	0.1
C <sub>6'''</sub>	0.220	0.462	0.011	0.1
C <sub>7'''</sub>	0.092	0.209	0.206	0.1
C <sub>8'''</sub>	0.040	0.190	0.419	0.1
C <sub>9'''</sub>	0.209	0.176	0.146	0.1
C <sub>10'''</sub>	0.150	0.088	0.108	0.1
C <sub>11'''</sub>	0.261	0.057	1.023	0.1
C <sub>12'''</sub>	0.333	0.196	0.292	0.1

<sup>a</sup>C<sub>1</sub>–C<sub>12</sub>: atoms of chain iP(R)-3MP-L-G<sup>+</sup>T (down); C<sub>1'</sub>–C<sub>12'</sub>: atoms of iP(S)-3MP-R-G<sup>+</sup>T (up); C<sub>1''</sub>–C<sub>12''</sub>: atoms of iP(R)-3MP-R-G<sup>+</sup>T (up); C<sub>1'''</sub>–C<sub>12'''</sub>: atoms of iP(S)-3MP-L-TT (down).

the calculated patterns of the models for the space group  $P2_1/b$ . The presence of this reflection with  $k$  odd suggests that in the very local arrangement of chains the symmetry of the space group should be lower than  $P2_1/b$  and that locally, the glide

plane symmetry  $b$  is not present. A possible space group that describes the very local packing of chains could be  $P2_1$ . A limit disordered model of packing with chains arranged as in the model of Figure 14 but with space group symmetry  $P2_1$  is shown in Figure 16. In this model the two chains included in

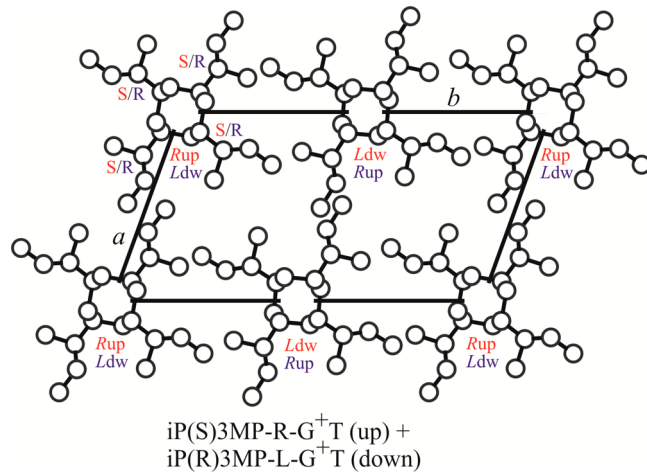


**Figure 16.** Limit disordered model of packing of iP(R,S)3MP in the monoclinic unit cell with axes  $a = 10.02 \text{ \AA}$ ,  $b = 18.48 \text{ \AA}$ ,  $c = 6.87 \text{ \AA}$ , and  $\gamma = 109.9^\circ$  according to the space group  $P2_1$ . The two chains included in the unit cell at  $y = 0$  and  $0.5$  are independent; that is, they are not related by elements of symmetry and are assumed to be enantiomorphous and anticlined, as in the model  $P2_1/b$  of Figure 14, but with independent settings  $\omega$  and  $z$ . The lattice site at  $x = y = 0$  is occupied with the same probability by chains iP(S)3MP-R-G<sup>+</sup>T (up) (chain model of Figure 7C) and iP(R)3MP-L-G<sup>+</sup>T (down) (chain model of Figure 7F), having opposite chirality in the helical hand (right-handed and left-handed), opposite S and R chirality of the lateral groups, and opposite up and down orientation (anticlined chains). The chains iP(S)3MP-R-G<sup>+</sup>T (up) and iP(R)3MP-L-G<sup>+</sup>T (down) have identical projections in the  $ab$  plane.

the unit cell with chain axes at  $y = 0$  and  $y = 0.5$  are independent; that is, they are not related by elements of symmetry (in the model of Figure 14 these chains at  $y = 0.25$  and  $0.75$  are related by the glide plane  $b$ ). In the model of Figure 16 the two chains are assumed to be enantiomorphous and anticlined, as in the model  $P2_1/b$  of Figure 14, but with independent settings  $\omega$  and  $z$ . Also in this model each site of the crystalline lattice is occupied with the same probability by chains iP(S)3MP-R-G<sup>+</sup>T (up) (chain model of Figure 7C) and iP(R)3MP-L-G<sup>+</sup>T (down) (chain model of Figure 7F), having opposite chirality in the helical hand (right-handed and left-handed), opposite S and R chirality of the lateral groups, and opposite up and down orientation (anticlined chains). The structure factors calculated for the limit disordered model of Figure 16 for the space group  $P2_1$  are reported in Table S5 (for powder diffraction) and Table S6 (for fiber diffraction) of the Supporting Information, whereas the calculated powder diffraction profile is reported in Figure 12B (profile g) and the calculated fiber diffraction pattern is shown in Figure 13G. A good agreement is obtained also for this low symmetry model with a value of the disagreement factor  $R$  of 18%. Additional types of disorder could also be present, as disorder in the conformation of the lateral groups and in the azimuthal setting of the chains around the chain axes and in the relative shift of the chains along  $c$ , compatible with the  $P2_1$  space group symmetry.

## CONCLUSIONS

Isotactic poly((*R,S*)-3-methyl-1-pentene) (iP(*R,S*)3MP) has been prepared by hydrogenation of isotactic 1,2-poly(*E*-3-methyl-1,3-pentadiene) which in turn has been synthesized with a new class of catalysts based on cobalt phosphine complexes of the type  $\text{CoCl}_2(\text{PMeRPh}_2)_2$ . The synthetic strategy based on hydrogenation route has allowed for the preparation of a purely statistical copolymer of the two enantiomeric monomers, with compensation of chirality.

The crystal structure of the random copolymer iP(*R,S*)3MP has been determined by analysis of the X-ray powder and fiber diffraction patterns and conformational and packing energy calculations. Chains in 4/1 helical conformation are packed in a monoclinic unit cell with parameters  $a = 10.02 \text{ \AA}$ ,  $b = 18.48 \text{ \AA}$ ,  $c = 6.87 \text{ \AA}$ , and  $\gamma = 109.9^\circ$  according to the space group  $P2_1/b$  or  $P2_1$ . A high degree of disorder is present in the crystals due to the random enchainment of the enantiomeric *R* and *S* monomeric units, whose chirality influences the handedness of the helical chains and the conformation assumed by the lateral groups. Disorder in the conformation of the lateral groups is therefore also present. In the crystals chain stretches of sequences of monomeric units in a prevailing *S* configuration tend to assume right-handed 4/1 helical conformations (combination *S*-right), whereas sequences of monomeric units in a prevailing *R* configuration tend to assume left-handed 4/1 helical conformation (combination *R*-left). Left-handed 4/1 helices for sequences of *S* monomers and right-handed helices for sequences of *R* monomers are also possible at a low cost of internal energy. In all cases the side groups are characterized by high degree of conformational disorder, due to the low energy barrier between the different rotational states. Disorder in the substitution of 4/1 helices of different chirality (right- and left-handed) in each site of the lattice is also present. Some kind of azimuthal disorder in the relative rotation of the chains around the chain axes, compatible with the  $P2_1/b$  or  $P2_1$  space group symmetry, may also be present.

The crystal structure of the random copolymer iP(*R,S*)3MP is different from that of the chiral pure enantiomer iP(*S*)3MP that is characterized by the isochiral packing of chains in 4/1 helical conformation in a tetragonal unit cell, according to the space group  $I4_1$ . The tetragonal crystal packing for iP(*S*)3MP is in agreement with the simple principle of packing of polymer chains in 4/1 helical conformations.<sup>10</sup> The crystal structure of iP(*R,S*)3MP is an example of *symmetry breaking* since chains in 4/1 helical conformation are not packed in a tetragonal lattice, but in a monoclinic lattice and the local symmetry of the chains is lost in the lattice. The different packing modes in the chiral and achiral isomers are driven by different entropic effects related to different types of disorder. In the structure of the pure chiral enantiomer iP(*S*)3MP, the entropic effect arising from the two possible conformational states assumed by the chiral lateral groups prevails and induces crystallization of isochiral helices.<sup>3,10</sup> In the case of the achiral random copolymer iP(*R,S*)3MP the entropic effect due to the statistical substitution of helices of different chirality and clinicity prevails and induces crystallization of antichiral monoclinic structure.

## ASSOCIATED CONTENT

### Supporting Information

Details of experimental data of polymer synthesis, solution NMR analysis, polymer characterization, and details of conformational and packing energy calculations, and of

structure factors calculations. The Supporting Information is available free of charge on the ACS Publications website at DOI: 10.1021/acs.macromol.5b00921.

## AUTHOR INFORMATION

### Corresponding Author

\*Tel ++39 081 674346; Fax ++39 081 674090; e-mail claudio.derosa@unina.it (C.D.R.).

### Notes

The authors declare no competing financial interest.

## ACKNOWLEDGMENTS

Financial support from “Ministero dell’Istruzione, dell’Università e della Ricerca” (project PRIN 2010-2011 and project PON-DIATEME 2007-2013) is gratefully acknowledged.

## REFERENCES

- (1) Pino, P.; Ciardelli, F.; Lorenzi, G. P.; Montagnoli, G. *Makromol. Chem.* **1963**, *61*, 207. Pino, P. *Adv. Polym. Sci.* **1965**, *4*, 393. Pino, P.; Lorenzi, G. P. *J. Am. Chem. Soc.* **1960**, *82*, 4745. Luisi, P. L.; Pino, P. *J. Phys. Chem.* **1968**, *72*, 2400.
- (2) Bassi, I. W.; Bonsignori, O.; Lorenzi, G. P.; Pino, P.; Corradini, P.; Temussi, P. A. *J. Polym. Sci. A2* **1971**, *9*, 193.
- (3) Petraccone, V.; Ganis, P.; Corradini, P.; Montagnoli, G. *Eur. Polym. J.* **1972**, *8*, 99.
- (4) Green, M. M.; Park, J. W.; Sato, T.; Teramoto, A.; Lifson, S.; Selinger, R. L. B.; Selinger, J. V. *Angew. Chem., Int. Ed.* **1999**, *38*, 3138.
- (5) Natta, G.; Pino, P.; Mazzanti, G.; Corradini, P.; Giannini, U. *Rend. Accad. Naz. Lincei (VIII)* **1955**, *19*, 397.
- (6) Pino, P.; Ciardelli, F.; Montagnoli, G. *J. Polym. Sci., Part C* **1968**, *16*, 3265.
- (7) Oliva, L.; Longo, P.; Zambelli, A. *Macromolecules* **1996**, *29*, 6383.
- (8) Allegra, G.; Corradini, P.; Ganis, P. *Makromol. Chem.* **1966**, *90*, 60.
- (9) Corradini, P.; Petraccone, V.; Pirozzi, B. *Eur. Polym. J.* **1976**, *12*, 831.
- (10) De Rosa, C.; Auriemma, F. *Crystals and Crystallinity in Polymers*; Wiley: Hoboken, NJ, 2014.
- (11) (a) Ricci, G.; Forni, A.; Boglia, A.; Motta, T.; Zannoni, G.; Canetti, M.; Bertini, F. *Macromolecules* **2005**, *38*, 1064. (b) Ricci, G.; Forni, A.; Boglia, A.; Sommazzi, A.; Masi, F. *J. Organomet. Chem.* **2005**, *690*, 1845.
- (12) Ricci, G.; Leone, G.; Boglia, A.; Bertini, F.; Boccia, A. C.; Zetta, L. *Macromolecules* **2009**, *42*, 3048.
- (13) Harwood, H. J.; Russel, D. B.; Verthe, J. J. A.; Zymonas, J. *Makromol. Chem.* **1973**, *163*, 1. Mango, L. A.; Lenz, R. W.; Zymonas, J. *Makromol. Chem.* **1973**, *163*, 13.